Clim. Past Discuss., 8, 6135–6198, 2012
www.clim-past-discuss.net/8/6135/2012/
doi:10.5194/cpd-8-6135-2012

Climate of the Past Discussions

Millennial-scale variability of marine productivity and terrigenous matter supply in the western Bering Sea over the past 180 kyr

J.-R. Riethdorf[1,*], D. Nürnberg[1], L. Max[2], R. Tiedemann[2], S. A. Gorbarenko[3], and M. I. Malakhov[4]

[1]Helmholtz Centre for Ocean Research Kiel (GEOMAR), Wischhofstr. 1-3, 24148 Kiel, Germany
[2]Alfred Wegener Institute for Polar and Marine Research, Am Handelshafen 12, 27570 Bremerhaven, Germany
[3]Pacific Oceanological Institute, Far Eastern Branch, Russian Academy of Sciences, Baltiskaya St. 43, 690041 Vladivostok, Russia
[4]North Eastern Interdisciplinary Science Research Institute (NEISRI), Far Eastern Branch, Russian Academy of Sciences, Portovaya St. 16, 685000 Magadan, Russia
[*]now at: Department of Ocean Floor Geoscience, Atmosphere and Ocean Research Institute, University of Tokyo, 5-1-5 Kashiwanoha, Kashiwa, Chiba 277-8564, Japan

Received: 29 November 2012 – Accepted: 4 December 2012 – Published: 12 December 2012

Correspondence to: J.-R. Riethdorf (jriethdorf@geomar.de)

Published by Copernicus Publications on behalf of the European Geosciences Union.

Abstract

We used piston cores recovered in the western Bering Sea to reconstruct millennial-scale changes in marine productivity and terrigenous matter supply over the past ~180 kyr. Based on a geochemical multi-proxy approach our results indicate closely interacting processes controlling marine productivity and terrigenous matter supply comparable to the situation in the Okhotsk Sea. Overall, terrigenous inputs were high, whereas primary production was low. Minor increases in marine productivity occurred during warm intervals of stage 5 and interstadials, but pronounced maxima were recorded during interglacials and Termination I. Seasonal sea-ice is suggested to act as the dominant transport agent for terrigenous material. From our results we propose glacial, deglacial, and interglacial scenarios for environmental change in the Bering Sea. These changes seem to be primarily controlled by insolation and sea-level forcing which affect the strength of atmospheric pressure systems and sea-ice growth. The opening history of the Bering Strait and the Aleutian passes is considered to have had an additional impact. Sea-ice dynamics are thought to drive changes in surface productivity, terrigenous inputs, and upper-ocean stratification. High-resolution core logging data (color b*, XRF scans) strongly correspond to the Dansgaard–Oeschger climate variability registered in the NGRIP ice core and support an atmospheric coupling mechanism of Northern Hemisphere climates.

1 Introduction

The subarctic North Pacific (N Pacific) is a high-nitrate, low-chlorophyll (HNLC) region (e.g. Kienast et al., 2004; Tyrrell et al., 2005), characterized by salinity-driven stratification (permanent halocline), which is suggested as a potential control mechanism of late Quaternary glacial/interglacial variations in atmospheric carbon dioxide (CO_2) concentrations (Haug et al., 1999, 2005; Sigman and Boyle, 2000; Sigman et al., 2004, 2010; Jaccard et al., 2005). The halocline prevents formation of deep water (Warren,

CPD
8, 6135–6198, 2012

1983; Emile-Geay et al., 2003) and modulates the supply of nutrient-rich deep water into the photic zone, thereby influencing the extent of marine productivity and nutrient utilization. Since the halocline also acts as a barrier for atmospheric-oceanic gas exchange, the modern N Pacific with its high carbon export efficiency (Honda et al., 2002) is considered a net sink of atmospheric CO_2 (Takahashi et al., 2002a).

Several studies have reported low marine productivity in the N Pacific during glacial times (Narita et al., 2002; Kienast et al., 2004; Jaccard et al., 2005, 2009, 2010; Brunelle et al., 2007; Shigemitsu et al., 2007; Galbraith et al., 2008; Gebhardt et al., 2008). However, it remains unclear, whether reduced marine productivity and low atmospheric CO_2 were caused by increased polar stratification or by enhanced sea-ice cover. Both processes would result in a less efficient biologically-driven drawdown of organic matter to the deep ocean and its subsequent degradation to CO_2 ("biological pump"), and hamper the release of deep-sequestered CO_2 to the atmosphere. Interglacial maxima in export productivity at ODP Site 882 were related to reduced stratification rather than to sea-ice influence (Jaccard et al., 2005). Since the modern Bering Sea is marked by high marine productivity and seasonal sea-ice formation (e.g. Springer et al., 1996; Niebauer et al., 1999) it might have had a different influence on past ocean-atmosphere CO_2 exchange. Paleoceanographic reconstructions also revealed reduced surface productivity during the last glacial period, which increased during Termination I and remained high in the Holocene (Gorbarenko, 1996; Cook et al., 2005; Gorbarenko et al., 2005; Okada et al., 2005; Okazaki et al., 2005; Brunelle et al., 2007, 2010; Itaki et al., 2009; Khim et al., 2010; Kim et al., 2011). This variability was explained by a complex interplay of changes in sea surface temperatures (SST), sea-ice extent, inflow of Pacific surface waters, and upper-ocean stratification (e.g. Katsuki and Takahashi, 2005; Brunelle et al., 2007, 2010; Kim et al., 2011).

Knowledge of past sea-ice variability in the Bering Sea comes from diatom and radiolarian assemblages, and IP_{25} biomarker studies (Cook et al., 2005; Katsuki and Takahashi, 2005; Tanaka and Takahashi, 2005; Max et al., 2012). Although sea-ice is considered an important transport agent for terrigenous material, geochemical or

CPD
8, 6135–6198, 2012

sedimentological studies assessing past terrigenous matter supply are rare. Existing studies focused on the Okhotsk Sea (Sato et al., 2002; Nürnberg and Tiedemann, 2004; Nürnberg et al., 2011) and the Southern Ocean (Latimer and Filippelli, 2001). For the Okhotsk Sea Nürnberg and Tiedemann (2004) suggested that nearly synchronous glacial/interglacial changes in biological and terrigenous fluxes were modulated by sea-ice processes driven by variations in the strength of the Siberian High. For the Bering Sea some provenance studies involving sedimentological and geochemical characteristics of surface sediments are available (Gardner et al., 1980; Lisitzin, 2002). However, downcore records reflecting the compositional variability of terrigenous matter are missing.

Recent progress has been made in detecting millennial-scale climate variability in Bering Sea sediments (Cook et al., 2005; Gorbarenko et al., 2005, 2010; Okazaki et al., 2005; Brunelle et al., 2010; Khim et al., 2010; Kim et al., 2011; Max et al., 2012; Rella et al., 2012). Most of these studies are restricted to the last ~ 70 kyr or focus on deglacial changes in the northern, southern, and southeastern Bering Sea. Together with studies from the NE Pacific (e.g. Hendy and Kennett, 2000) they imply that short episodes of increased marine productivity are connected with interstadials recorded in Greenland ice cores. However, existing reconstructions are constrained by the shallow lysocline within the N Pacific realm limiting the use of carbonate-based proxies and causing stratigraphic uncertainties. In the Bering Sea according reconstructions are restricted to shallow shelf areas or morphological highs. Here, we present millennial-scale reconstructions of marine productivity and terrigenous matter supply for the hitherto only poorly studied western Bering Sea. Results were derived from a suite of geochemical proxies and high-resolution core logging data covering the last ~ 180 kyr.

2 Regional setting

The Bering Sea links the Pacific Ocean with the Arctic Ocean via the only shallow (~ 50 m) Bering Strait. In its eastern and northern part it is characterized by a wide

CPD
8, 6135–6198, 2012

and shallow (0–200 m) continental shelf area. Pacific surface waters, transported by the westward flowing Alaskan Stream, enter the Bering Sea through several passes within the Aleutian Island Arc (e.g. Takahashi, 2005). Inside the Bering Sea, a large-scale cyclonic surface circulation pattern develops with the Bering Slope Current and the East Kamchatka Current acting as eastern and western boundary currents, respectively (Fig. 1). Outflow occurs through Bering Strait into the Arctic Ocean and through the Aleutian passes, mainly Kamchatka Strait, into the N Pacific (Stabeno et al., 1999). Deep waters flow northward and eastward from Kamchatka Strait with return outflow above 3000 m water depth (Reed et al., 1993; Stabeno et al., 1999). Oceanographic and climatic conditions are characterized by a strong seasonal variability of SST and sea-ice coverage that result from the interaction of the Siberian High and Aleutian Low. The Arctic Oscillation, Pacific Decadal Oscillation, and the Pacific–North American pattern are reported to be related with decadal variations of both atmospheric pressure cells (Niebauer, 1988, 1998; Mantua et al., 1997; Overland et al., 1999, 2002). During winter, a strong Siberian High leads to advection of cold Arctic air masses and mainly northerly wind directions (Stabeno et al., 1999). This causes a significant cooling of the sea surface, sea-ice formation, as well as enhanced vertical mixing in the mixed layer, thereby returning nutrients from the subsurface. In contrast, during summer, the reduced strength of the Aleutian Low and enhanced insolation result in a stratified mixed layer and increased marine productivity.

Primary productivity is dominated by diatoms mainly blooming during spring, whereas increased biological $CaCO_3$ fluxes (coccolithophores, planktonic foraminifera) occur during spring and late summer/early fall (e.g. Takahashi et al., 2002b). Highest annual production rates are associated with shelf areas and vary regionally between >200 and $>800\,g\,C\,m^{-2}$ (Arzhanova et al., 1995; Springer et al., 1996; Stabeno et al., 1999). Available nutrients are reported to be often fully consumed during seasonal blooms (Niebauer et al., 1995).

Sea-ice formation begins during October/November on the northern Bering Sea continental shelf (Anadyr Bay, Bering Strait), reaching maximum distribution in March/April,

CPD
8, 6135–6198, 2012

subsequently disintegrating until July (Tomczak and Godfrey, 1994; Niebauer et al., 1999; Lisitzin, 2002). It takes place in shallow shelf areas, bays, and coastal areas. As in the Arctic, coastal polynyas play an important role for the build-up of sea-ice, and consequently for water mass ventilation due to brine rejection (Niebauer et al., 1999; Stabeno et al., 1999). Processes entraining sediment into newly formed ice involve tidal sea-level oscillations, wind mixing, resuspension of sediments from the seafloor (suspension freezing), beach-ice formation, nearshore anchor ice formation, and seabed freezing (e.g. Nürnberg et al., 1994, 2011, and references therein; Stein, 2008, and references therein). Especially during fall and winter, storms affect reworking and resuspension processes by sea-ice crushing, mixing of the water column, and detachment of the sediment-laden ice from the coast. The sediment freight is released by sea-ice melting, especially during spring/summer, and then contributes to (hemi-) pelagic sedimentation.

3 Material and methods

This study is based on piston cores SO201-2-77KL, -85KL, and -101KL from Shirshov Ridge, western Bering Sea (Fig. 1, Table 1). Cores were recovered along a ~280 km-long north-south transect from shallow to deep intermediate water levels during R/V *Sonne cruise* SO201-KALMAR Leg 2 in 2009 (Dullo et al., 2009). The sedimentary succession is characterized by monotonous sequences of mainly clay- and silt-sized siliciclastic material, which are repeatedly interrupted by layers of diatomaceous ooze. Except for the younger part of the Holocene, which mainly consists of diatom-rich sediment, our sediment cores contained sufficient carbonate to allow for high-resolution paleoceanographic reconstructions. However, in cores 85KL and 101KL sediments younger than 7.5 ka BP and 12.5 ka BP, respectively, are not preserved.

CPD
8, 6135–6198, 2012

3.1 Stratigraphic approach

3.1.1 Core logging

Color reflectance measurements were carried out using a Minolta CM 508d hand-held spectrophotometer at 1 cm-spaced intervals (Dullo et al., 2009). Reflectance data were automatically converted by Spectramagic software into CIE L*, a* and b* color space (CIELAB).

The Avaatech X-ray fluorescence (XRF) core scanner at Alfred Wegener Institute for Polar and Marine Research, Bremerhaven, was used to determine relative changes in the sedimentary elemental composition. Core scanning was performed on the split core surface covered with SPEX CertiPrep 3525 Ultralene foil (4 µm thick). Each core segment was triple-scanned for analysis of elements Al through Ba at 1 mA, but at different tube voltages and count times (10 kV, 10 s; 30 kV, 15 s; 50 kV, 30 s), using a sampling resolution of 1 cm. Results are considered semiquantitative (Richter et al., 2006; Tjallingii et al., 2007) and are given as count rates (in cps) or as log-ratios (natural logarithm) of element count rates.

3.1.2 Stable oxygen isotopes

For stable oxygen isotope (δ^{18}O) stratigraphy we used endobenthic foraminifer species *Uvigerina peregrina* and *Uvigerina auberiana*, since *Uvigerina* δ^{18}O values are reported to be in equilibrium with seawater (Shackleton and Hall, 1984). δ^{18}O was measured every 5 cm on 2–3 tests of *U. peregrina*, or, if not present, of *U. auberiana*, collected from the 315–355 µm size fraction. Measurements were performed at GEOMAR, Kiel, using a Thermo Finnigan MAT253 mass spectrometer coupled with a Thermo Scientific Kiel IV Carbonate device. Results were referenced to the NBS19 standard and calibrated to the VPDB scale. Long-term precision ($n > 1000$ samples) for δ^{18}O of the used carbonate standard (Solnhofen limestone) was ± 0.06 ‰. In core 77KL benthic foraminifera were only preserved until 865 cm core depth.

CPD
8, 6135–6198, 2012

3.1.3 Paleomagnetics

Sedimentary natural remanent magnetization (NRM) was determined in core 85KL based on saturation magnetization in magnetic-hysteresis parameters, and by differential thermomagnetic analyses using a Faraday magnetic balance and a coercive spectrometer (Burov et al., 1986; Yasonov et al., 1998). The NRM module and direction were measured with a AGICO JR-5A spinner magnetometer after the stepwise demagnetization of a reference sample. Magnetic cleaning was performed using an alternating magnetic field with an amplitude of 10 mT to recognize the characteristic component of NRM (ChRM). Anhysteretic remanent magnetization (ARM) was generated in the preliminarily demagnetized samples using a AGICO AMU-1A anhysteretic magnetizer under a constant field of 0.05 mT and a maximum alternating field of 100 mT. Relative paleointensity of the magnetic field (RPI) was then calculated by normalization of ChRM to ARM. Scalar petromagnetic properties (SPP) were additionally determined (Enkin et al., 2007; Malakhov et al., 2009). All measurements were conducted at NEISRI, Magadan.

3.1.4 Age models

The chronostratigraphic approach included high-resolution core logging data (color b*, XRF scanning), benthic δ^{18}O stratigraphy, magnetostratigraphy, and accelerator mass spectrometry (AMS) radiocarbon dating of planktonic foraminifera for absolute age control. A detailled presentation of the stratigraphic framework for the last 20 kyr, including the AMS-^{14}C dating results, is provided in Max et al. (2012). The pre-deglacial (> 20 ka BP) stratigraphic framework of our cores is primarily based on the graphic correlation between color b* recorded in core 85KL and the Dansgaard–Oeschger (D-O) climate variability registered in the NGRIP δ^{18}O record (NGRIP members, 2004; GICC05 timescale, Rasmussen et al., 2006) (Fig. 2a). For ages > 122 ka BP and for identification of the Marine Isotope Stage (MIS) 5.5 climate optimum (~ 125 ka BP) color b* and XRF Ca/Ti log-ratios were correlated to the Sanbao stalagmite δ^{18}O

CPD
8, 6135–6198, 2012

record (Wang et al., 2008). The Laschamp (~42 ka BP), Norwegian–Greenland Sea (~65 ka BP), and Blake (~117 ka BP) paleomagnetic excursions were identified in the RPI record and correlated with the PISO-1500 geomagnetic paleointensity stack (Channell et al., 2009). Further ages were derived from comparison of benthic $\delta^{18}O$ values and SPP (not shown) with the global reference stack LR04 (Lisiecki and Raymo, 2005), which was also used to identify boundaries of stages 1 to 6. The stratigraphy of core 85KL was transferred via intercore correlations (color b*, XRF Ca/Ti log-ratios) to cores 77KL and 101KL (Fig. 2b), for which similar stratigraphic approaches were carried out. All age-depth points are provided in Appendix A.

Figure 3 shows the age models for our cores by direct comparison with the used reference records and a respective age versus depth diagram. Age models were tested via spectral analysis of the color b* and benthic $\delta^{18}O$ records in the time domain to detect orbital frequencies. Spectral analysis was performed using the AnalySeries 2.0 software (Paillard et al., 1996). Despite the shortness of our records with respect to orbital-scale changes, we found dominant cyclicities of ~23 and ~39 kyr, which within appropriate bandwidths match frequencies of orbital precession ($0.047 \pm 0.005\,kyr^{-1}$) and obliquity cycles ($0.025 \pm 0.0015\,kyr^{-1}$) (Fig. 3).

3.2 Sedimentation and accumulation rates

Linear sedimentation rates (LSR, in $cm\,kyr^{-1}$) were calculated between age control points and bulk accumulation rates (AR_{Bulk}, in $g\,cm^{-2}\,kyr^{-1}$) were calculated as the product of LSR and the dry bulk density (DBD, in $g\,cm^{-3}$). DBD was determined each 5 cm. Records of LSR and AR_{Bulk} are shown in Fig. 4. Cores from Shirshov Ridge have average LSR (AR_{Bulk}) of 11–16 $cm\,kyr^{-1}$ (7–15 $g\,cm^{-2}\,kyr^{-1}$), and hence allow for centennial- to millennial-scale reconstructions. Variability and average values of LSR and AR_{Bulk} increase towards the northernmost site. In general, LSR and AR_{Bulk} are higher during cold intervals (stages 6, 5.4, 5.2, and 4) than during warm intervals (stages 5.5, 5.3, 5.1, 3, and 1), but highest during Termination I (20–10 ka BP) (Fig. 4).

CPD
8, 6135–6198, 2012

Holocene sediments are either not preserved or subject to low LSR (AR_{Bulk}). We consider this to be the result of a change in sedimentation favoring the deposition of highly porous diatomaceous ooze, since piston cores are reported to rather cause oversampling (stretching) of the sediments (Széréméta et al., 2004) and because the piston should have prevented sediment loss during coring.

In this study, we report proxy concentrations rather than quantified flux rates and treat the respective records as qualitative. Accumulation rates in contrast to proxy concentrations are unaffected by depositional dilution or enrichment. However, if proxy concentrations in marine sediments cores are low or vary only little, the variability of accumulation rates mainly reflects the LSR variability (Middelburg et al., 1997). This situation applied to our sediment cores.

3.3 Assessment of marine productivity

Past changes in marine productivity were approximated from total organic carbon (TOC), $CaCO_3$, biogenic opal, biogenic barium (Ba_{bio}), and XRF logging data. This multi-proxy approach was necessary due to specific restrictions of the respective proxies. TOC preservation in sediments is highly debated (e.g. Hartnett et al., 1998; Ganeshram et al., 1999; Thunell et al., 2000; Hedges et al., 2001) as it is, e.g. influenced by oxidation processes and bottom water ventilation (De La Rocha, 2007). Also, its source can be of marine and terrigenous origin. In the N Pacific the preservation of $CaCO_3$ is limited by the shallow lysocline. Accordingly, $CaCO_3$ concentrations rather reflect changes in the bottom water calcite saturation state (e.g. Jaccard et al., 2005; Gebhardt et al., 2008). Opal dissolves during settling to the seafloor, but its preservation is independent from bottom water oxygenation. Since opal-rich sediments are linked to biogenic silica production (e.g. Nelson et al., 1995; Ragueneau et al., 2000; Pondaven et al., 2000; Matul et al., 2002) biogenic opal is most often used in N Pacific reconstructions of marine productivity. Barium, present as sedimentary barite is used in several studies to reconstruct paleoproductivity (e.g. Dymond et al., 1992; Francois et al., 1995; Dymond and Collier, 1996; Gingele et al., 1999), although evidence for

CPD
8, 6135–6198, 2012

direct biogenic barite formation does not exist. Barite particles occur in areas of high new production (Dehairs et al., 1991).

3.3.1 CN-analyses and biogenic opal

Total carbon (TC), TOC, and total nitrogen (TN) were determined on freeze-dried bulk sediment samples of 20 mg using a Carlo Erba NA-1500 CNS analyzer. TOC was measured on previously decalcified samples and $CaCO_3$ concentrations were calculated by multiplication of the difference between TC and TOC with a factor of 8.333. Reproducibility of the TOC and TN measurements was ± 0.03 wt. % and ± 0.01 wt. %, respectively.

The atomic ratio of TOC to TN, corrected for inorganic nitrogen compounds ([C/N]a), was used to distinguish between marine and terrigenous sources of TOC. The Redfield ratio (Redfield et al., 1963) translates the C/N ratio of marine organic matter to ~ 7. Typical terrigenous values lie between 20–200 (Hedges et al., 1986). We applied a correction for total inorganic nitrogen (TIN), usually clay-bound inorganic ammonium (Müller, 1977), based on a linear relationship between TOC and TN (after Goñi et al., 1998). Results showed TIN concentrations of 0.01–0.02 wt. % that were assumed constant downcore.

Biogenic opal was measured following Müller and Schneider (1993) using molybdate-blue spectrophotometry. Silica was extracted from 20 mg of freeze-dried bulk sediment samples. Results were evaluated applying the procedure of DeMaster (1981). Replicate measurements showed a reproducibility of 1–2 wt. %.

3.3.2 Biogenic barium (Ba_{bio})

Concentrations of major (Al, Ti, Fe, K) and trace (Ba) elements were determined from 0.6 g of freeze-dried bulk sediment using a Philips PW1480 XRF spectrometer without determination of loss on ignition following standard procedures. Analytical precision, determined for the BHVO standard, was < 2 % RSD for the major elements and

CPD
8, 6135–6198, 2012

± 30 ppm for Ba (N = 15). Results for barium (Ba_{total}) are the sum of biogenic (Ba_{bio}) and nonbiogenic Ba-portions. Ba_{bio} was therefore calculated via concentrations of Al by estimating the aluminosilicate contribution of Ba considering the global average Ba/Al ratio for pelitic rocks of 6.5 mg g^{-1} (Wedepohl, 1971):

$$Ba_{bio} = Ba_{total} - Al \times 0.0065 \quad (1)$$

Ba_{bio} was subsequently used to assess new production (P_{New}) by applying the relationship of Nürnberg (1995). Annual primary production (PP) was calculated after Eppley and Peterson (1979) using P_{New}.

3.3.3 XRF logging data (Br, Ca/Ti, Si/Al)

Several logging data and bulk geochemical analyses showed a similar temporal evolution. In this respect, XRF count rates of Br correlated with TOC concentrations ($0.35 < R^2 < 0.74$), which supports a relationship between TOC and biophilic halogen bromine (Ziegler et al., 2008). XRF Ca/Ti log-ratios correlated with $CaCO_3$ concentrations ($0.07 < R^2 < 0.65$), which is explained by assuming a detrital origin of Ti. Normalization of XRF-derived Ca to Ti and/or Al abundances has been applied before (Jaccard et al., 2005) and is thought to reflect biogenic $CaCO_3$ contents within the sediment. The XRF signals for Al were better than for Ti and were subsequently used for normalization. However, we favored Ca/Ti over Ca/Al log-ratios due to better correlation to $CaCO_3$. Although opal concentrations were close to reproducibility for most samples, they correlated with color b* ($0.20 < R^2 < 0.60$) and XRF Si/Al log-ratios ($0.04 < R^2 < 0.73$). This is in accordance with other studies considering a connection between Si/Al ratios and biogenic opal (McDonald et al., 1999). All linear relationships found are considered significant for cores 77KL and 85KL ($0.57 < R^2 < 0.74$), but insignificant for core 101KL ($0.04 < R^2 < 0.35$). Since the significance of the correlations varied between both, the respective sites and the respective proxies, the logging data were not used to apply calibration functions, but are shown together with the quantitative results.

CPD
8, 6135–6198, 2012

3.4 Assessment of terrigenous matter supply

3.4.1 Coarse material, siliciclastics, and terrigenous matter

Changes in terrigenous fluxes were approximated from a set of sedimentological and geochemical proxies together with XRF logging data. The proportions of coarse (> 63 µm) and fine (< 63 µm) material (in wt. %) were determined every 5 cm. Magnetic susceptibility (not shown) was logged using a GEOTEK Multi-Sensor Core Logger in combination with a Bartington MS2C sensor loop each 1 cm on the unopened core segments directly after recovery (Dullo et al., 2009). Records of > 63 µm did not match magnetic susceptibility records ($R^2 < 0.13$), which showed only low values (< 15 SI units). Hence, magnetizable minerals are mainly bound to the fine fractions.

Relative amounts of siliciclastics (%Siliciclastics) were calculated by considering the bulk sediment to be composed of siliciclastics, $CaCO_3$, TOC, and biogenic opal. TN concentrations were generally < 0.3 wt. % and not included in the calculation:

$$\%\text{Siliciclastics} = 100\,\% - (CaCO_3\,\% + \text{TOC}\% + \text{Opal}\%) \quad (2)$$

In a second approach, relative amounts of terrigenous matter (%Terrigen) were calculated by normalizing bulk sedimentary Al and Ti concentrations to their concentration in average continental crust (Al = 3117 µmol g^{-1}, Ti = 112.8 µmol g^{-1}; Taylor and McLennan, 1995). Both normalizations resulted in a similar temporal evolution of the records, but Al-normalized results, which were on average 4–6 % higher than Ti-normalized results, better compared to the records of %Siliciclastics.

3.4.2 Lithogenous elements

The geochemistry of lithogenous elements can be used to approximate continental input (e.g. Duce and Tindale, 1991; Bareille et al., 1994), dust-supply (e.g. Boyle, 1983; Calvert and Fortugne, 2001), terrestrial runoff (e.g. Schmitz, 1987; Jansen et al., 1998), and mineralogical variations (e.g. Schneider et al., 1997; Yarincik et al., 2000). We used

CPD
8, 6135–6198, 2012

XRF bulk analyses of elements Al, Ti, Fe, and K and their respective ratios to identify sources of terrigenous matter and to reconstruct variations in terrigenous fluxes. In cores 85KL and 101KL XRF logging data of K/Ti log-ratios correlated well with atomic K/Ti ratios ($R^2 > 0.64$) and are shown for comparison.

4 Results and discussion

4.1 Marine productivity

4.1.1 Proxy data

Productivity proxies show a similar temporal evolution in all cores, but increasing proxy concentrations towards the southernmost site. Results for TOC, opal, $CaCO_3$, as well as their approximating logging data are shown in Fig. 5. In general, marine productivity remained low during cold (stages 6, 5.4, 5.2, 4, and 2), but high during warm intervals (stages 5.5, 5.3, 5.1, and 1), with maximum values recorded during interglacials in core 77KL. Core 101KL exhibits lowest proxy concentrations and amplitude variations (Table 2). Overall concentrations hardly exceed ~1 wt.% for TOC, ~3 wt.% for opal, and ~2 wt.% for $CaCO_3$. Stages 5.3 and 5.1, as well as interstadials are characterized by ~1 to 3-times higher values at most. Notably, cores 85KL and 101KL recorded interstadial-like events during stage 6 (at ~173 ka BP, 164 ka BP, 148 ka BP, 137 ka BP, and 133 ka BP), characterized by increased proxy concentrations or their approximating XRF data. Deglacial and interglacial maxima in TOC, opal, and $CaCO_3$ reach values of ~2 wt.%, ~50 wt.%, and ~30 wt.%, respectively. Maxima recorded during Termination I reflect the warm phases of the Bølling-Allerød (B/A; 14.7–12.9 ka BP, Blockley et al., 2012) and Preboreal (PB; ~11.7–11.0 ka BP), whereas deglacial minima are considered to correspond to the Heinrich Stadial 1 (H1; 18.0–14.7 ka BP, Sarnthein et al., 2001) and Younger Dryas cold phases (YD; 12.9–11.7 ka BP, Blockley et al., 2012).

CPD
8, 6135–6198, 2012

During Termination I, TOC appears to lead the deglacial increase of the other productivity proxies by ~2 kyr, which is in agreement with other Bering Sea studies (Gorbarenko, 1996; Okazaki et al., 2005; Kim et al., 2011). Although records of TOC and XRF count rates of Br correspond well in our cores (Fig. 5), Br does not follow this deglacial TOC-increase, suggesting a changing source of TOC. In contrast to TOC and $CaCO_3$, we observed only minor increases in opal during the B/A, but a subsequent gradual increase into the Holocene. These results are comparable to opal records from the northern slope (Itaki et al., 2009; Khim et al., 2010; Kim et al., 2011). Despite showing a similar temporal evolution, opal records from Bowers Ridge (Okada et al., 2005; Okazaki et al., 2005; Brunelle et al., 2007, 2010), Umnak Plateau (Okada et al., 2005; Okazaki et al., 2005), and the southern Okhotsk Sea (Gorbarenko, 1996; Gorbarenko et al., 2002a,b; Narita et al., 2002; Brunelle et al., 2010) have 1.5 to 3-times higher values. This further indicates decreasing, diatom-dominated marine productivity towards the northern Bering Sea.

$CaCO_3$ concentrations are generally low and related to the abundance of foraminifera and nannoplanktonic remains (coccoliths). High XRF Ca/Ti log-ratios during stage 5.5 originate from decreased XRF counts of Ti and not from increased Ca counts. Short-lived increases of up to ~3 wt.% were recorded during interstadials and stage 6 (Fig. 5). Similar observations were previously reported for Bering Sea cores (Cook et al., 2005; Okazaki et al., 2005; Brunelle et al., 2007, 2010; Itaki et al., 2009; Khim et al., 2010; Kim et al., 2011). At ODP Site 882 in the N Pacific interglacial maxima in $CaCO_3$ are accompanied by maxima in Ba_{bio} (Jaccard et al., 2005). Since enhanced preservation of $CaCO_3$ is explained by a release of deep sequestered CO_2 from the deep ocean basin (Broecker and Peng, 1987; Marchitto et al., 2005), these $CaCO_3$ maxima were suggested to be the result of a higher bottom water calcite saturation state in response to the weakening of the N Pacific halocline (Jaccard et al., 2005). Deglacial maxima of $CaCO_3$ in Bering Sea sediments were also explained by denitrification on continental shelves, which might have resulted in an increase in alkalinity and, thus, in enhanced carbonate preservation (Chen, 2002; Okazaki et al., 2005).

CPD
8, 6135–6198, 2012

Today, the calcite saturation horizon in the Bering Sea is reported to lie above 500 m water depth (Feely et al., 2002) and at our sites lies above 200 m water depth (Riethdorf et al., 2012). Accordingly, we consider $CaCO_3$ maxima in our cores to reflect a higher bottom water calcite saturation state.

4.1.2 Organic carbon source

[C/N]a ratios in our cores mainly vary between 10 and 15 (Fig. 6a, Table 2), indicating that TOC input contains mainly marine, but considerable amounts of terrestrial organic material. Strongest [C/N]a variability is observed at Site 77KL. All sites show a rise in [C/N]a ratios during Termination I, indicating enhanced supply of terrestrial matter. Since average concentrations of TN varied at ∼0.1 wt. %, sediments from Shirshov Ridge contain a considerable amount of TIN. Consequently, [C/N]a ratios are by up to 4 units higher than uncorrected ratios (Fig. 6a). Lower C/N ratios of 6–9 were reported for the eastern and southern part of the Aleutian Basin (Nakatsuka et al., 1995) and the southern Okhotsk Sea (Ternois et al., 2001). Our ratios are closer to those found at the northern slope (Khim et al., 2010) and the central Okhotsk Sea (Nürnberg and Tiedemann, 2004). At Site 77KL, the deglacial increase in [C/N]a ratios starts at ∼17 ka BP, with maximum values during the YD, and a subsequent decrease into the Holocene. The same deglacial evolution is observed at the northern slope (Khim et al., 2010) and in the southern Okhotsk Sea (Ternois et al., 2001; Seki et al., 2003). It was related to the discharge of terrestrial material from the flooded shelf due to sea-level rise. In contrast, cores from the eastern and southern Bering Sea show a gradual decrease of C/N ratios since the last glacial maximum (LGM) (Nakatsuka et al., 1995).

4.1.3 Ba_{bio} and export production

Records of Ba_{bio} are shown in Fig. 7 and overall match the TOC and opal records. A potential source of error in the calculation of Ba_{bio} comes from estimating the aluminosilicate contribution of Ba via Al. Ba/Al ratios range between 5–10 mg g^{-1} in crustal rocks

CPD
8, 6135–6198, 2012

(Taylor, 1964; Rösler and Lange, 1972) with a crustal average of 7.5 mg g^{-1} (Dymond et al., 1992). We estimated the regional detrital Ba/Al ratio from surface sediment samples following Klump et al. (2000), which resulted in a value of 7 mg g^{-1} (unpublished data). This value is close to the global average of pelitic rocks of 6.5 mg g^{-1} (Wedepohl, 1971), which was used for reconstructing Ba_{bio} in the central Okhotsk Sea (Nürnberg and Tiedemann, 2004). Ba_{bio} variability is low during most of the time covered by the cores, with average concentrations increasing from Site 101KL (~ 300 ppm), via Site 85KL (~ 400 ppm), to Site 77KL (~ 500 ppm) (Fig. 7, Table 2). Significant increases only occur at Site 77KL during stage 5.5 and the Holocene with concentrations of ~ 1000 ppm and ~ 1700 ppm, respectively. Also at Site 77KL, XRF Ba/Al log-ratios covary with Ba_{bio} concentrations (not shown; $R^2 = 0.74$), thereby showing minor increases during stages 5.3, 5.1, and during interstadials. A similar range and variability as found for core 77KL was observed at Bowers Ridge (Brunelle et al., 2007), ODP Site 882 (Jaccard et al., 2005), as well as the sea-ice-free Southern Ocean (Nürnberg et al., 1997). Cores from the southern (Brunelle et al., 2010) and central Okhotsk Sea (Sato et al., 2002; Nürnberg and Tiedemann, 2004), as well as from the sea-ice-influenced Southern Ocean (Nürnberg et al., 1997) exhibit generally lower glacial (~ 200–400 ppm) and peak interglacial (~ 800–1000 ppm) contents of Ba_{bio}, being more comparable to sites 85KL and 101KL. Notably, Sato et al. (2002) and Brunelle et al. (2010) for the Okhtosk Sea report a deglacial lead in the rise of Ba_{bio} prior to that observed for opal contents, which we can not verify from our records.

We calculated P_{New}, i.e. primary production that results from allochthonous nutrient inputs to the photic zone, from Ba_{bio} following Nürnberg (1995) rather than from TOC, which at our sites is affected by terrestrial carbon. Results show that export production during most of the last 180 kyr was commonly low (< 50 g C m^{-2} yr^{-1}) at all sites (Fig. 7, Table 2). Only core 77KL is characterized by two significant maxima > 150 g C m^{-2} yr^{-1} during Termination I. Although these maxima correspond to higher concentrations of Ba_{bio}, they might be overestimated due to the use of AR_{Bulk}. Nevertheless, our results are comparable to those reported for the central Okhotsk

CPD
8, 6135–6198, 2012

Sea (Nürnberg and Tiedemann, 2004) and the Antarctic continental margin (Gingele et al., 1999), albeit these show lower glacial values of $< 10\,g\,C\,m^{-2}\,yr^{-1}$. PP was estimated from P_{New} and mainly remains $< 150\,g\,C\,m^{-2}\,yr^{-1}$ (not shown). The deglacial maxima in core 77KL translate into PP-maxima of ~ 250–$300\,g\,C\,m^{-2}\,yr^{-1}$ (Table 2). Modern PP on the eastern Bering Sea shelf edge is reported to lie between 175–$275\,g\,C\,m^{-2}\,yr^{-1}$ (Springer et al., 1996). Stabeno et al. (1999) reported modern PP values of $> 200\,g\,C\,m^{-2}\,yr^{-1}$ over the southeastern shelf and $> 800\,g\,C\,m^{-2}\,yr^{-1}$ north of St. Lawrence Island, whereas Arzhanova et al. (1995) found $> 400\,g\,C\,m^{-2}\,yr^{-1}$ over the western shelf. Consequently, at Site 77KL modern PP values have only been reached since Termination I, whereas PP remained permanently low at sites 85KL and 101KL.

4.2 Terrigenous matter supply

4.2.1 Proxy data

Sediments from Shirshov Ridge are dominated by siliciclastic material. Light microscope observations reveal silt to fine sand-sized, angular-shaped quartz grains as major components, supplemented by minor portions of feldspar and mica. Coarse ice-rafted debris (IRD) and dropstones (1–2 cm in diameter) are commonly rare although occurring over the entire length of the cores. Proxy records exhibit a similar temporal evolution at all sites (Fig. 8), but in contrast to the productivity proxies decreasing concentrations towards the southernmost site are observed. In general, proxy records reflecting marine productivity and terrigenous matter supply are anticorrelated. Accordingly, cold intervals (stages 6, 5.4, 5.2, 4, and 2) are characterized by high terrigenous matter supply, whereas warm intervals (stages 5.5, 5.3, 5.1, and 1) show reduced proxy concentrations or ratios. Most pronounced minima are found during interglacials. In core 77KL higher amounts of $> 63\,\mu m$ and of $CaCO_3$ concentrations (XRF Ca/Ti log-ratios) occur synchronously, indicating that changes in $CaCO_3$ result from higher foraminiferal abundances. Although independently derived, covariation is also found

CPD
8, 6135–6198, 2012

between %Terrigen and %Siliciclastics, which are characterized by almost identical ranges (Fig. 8, Table 3).

Sediments contain on average > 85 % siliciclastics and only < 10 % coarse material (Table 3), thereby tying terrigenous matter mainly to the fine fractions. K/Ti ratios show a range of 5–7 mol mol^{-1} in all cores (Fig. 8, Table 3). We consider this ratio to be indicative of changes in the geochemical composition of the terrigenous matter. During stage 5.5 and the Holocene, %Siliciclastics are reduced to ~ 50 % at Site 77KL, ~ 60 % at Site 85KL, and ~ 70 % at Site 101KL. At the same time, K/Ti ratios decrease to ~ 5 mol mol^{-1}. Minor drops were recorded during stages 5.3 and 5.1 (~ 15 % in Siliciclastics; ~ 0.5 mol mol^{-1} in K/Ti), whereas K/Ti ratios increased by ~ 1 mol mol^{-1} during stage 4 and subsequently decreased during stage 3. In core 85KL stage 6 is characterized by pronounced maxima in XRF K/Ti log-ratios at ~ 173 ka BP and ~ 163 ka BP. This core and core 101KL reveal a minor peak in > 63 µm found at ~ 133 ka BP, which occurs simultaneously with minima in %Siliciclastics but with maxima in $CaCO_3$ and TOC. Notably, highest amounts of > 63 µm were recorded at sites 85KL and 101KL at the end of Termination II (~ 127–125 ka BP) with maxima of ~ 30 % and ~ 60 %, respectively. These maxima are concurrent with high [C/N]a ratios and lead maxima in opal concentrations by ~ 3 kyr. During Termination I, the B/A warm phase is characterized by reductions in %Siliciclastics and %Terrigen of up to ~ 25 % and of up to ~ 0.5 mol mol^{-1} in K/Ti. Maxima in > 63 µm were recorded during both, the B/A and the PB. Pronounced maxima in K/Ti are observed during the H1 cold phase. During the YD all proxies briefly return to glacial values, which is followed by a gradual decrease into the Holocene. The described proxy ranges and their temporal variability almost compare to those reported for the central Okhotsk Sea (Nürnberg and Tiedemann, 2004), except that respective sediment records showed even lower interglacial minima in %Siliciclastics of ~ 35 %.

In all cores significant linear correlations between concentrations of lithogenous elements Al, Fe, and Ti were found (Fig. 7). This indicates that these elements originate from the same geochemical source and/or share the same transport mechanism. [Al]

CPD
8, 6135–6198, 2012

correlated with %Siliciclastics in cores 77KL ($R^2 = 0.42$) and 85KL ($R^2 = 0.74$), but not in core 101KL ($R^2 = 0.08$). We consider an influence of scavenging by organic material and/or bottom sediment resuspension on [Al] (Orians and Bruland, 1986; Nameroff et al., 2004) insignificant, which is supported by low interglacial concentrations and Al/Ti ratios that are close to crustal values. Records for [Al], [Fe], and [Ti] follow the same temporal evolution described for the terrigenous proxies with general high values during most of the last 180 kyr ($\sim$2600–2800 µmol g^{-1} for [Al], $\sim$700–900 µmol g^{-1} for [Fe], $\sim$90–100 µmol g^{-1} for [Ti], Table 3). During stage 5.5 and the Holocene [Al], [Fe], and [Ti] decrease by up to $\sim$800 µmol g^{-1}, $\sim$300 µmol g^{-1}, and $\sim$30 µmol g^{-1}, respectively. From stage 3 to stage 1, [Fe] became slightly higher in core 77KL than in the other cores (Fig. 7). These results compare to those from the central Okhotsk Sea (Sato et al., 2002) and the Southern Ocean (Latimer and Filippelli, 2001). However, these studies reported on glacial [Al] and [Ti] that were by $\sim$30 % lower than those recorded at Shirhov Ridge. Moreover, these studies described very low interglacial values ($\sim$100 µmol g^{-1} for [Al], $\sim$100 µmol g^{-1} for [Fe], $\sim$10–20 µmol g^{-1} for [Ti]) not found at our sites. This argues for an interglacial reduction in terrigenous fluxes at Shirshov Ridge of only 30–40 %.

4.2.2 Geochemical signature

Atomic Al/Ti and Fe/Al ratios were used to characterize the geochemical signature of the sediments. In general, Al/Ti and Fe/Al ratios remained fairly constant during the last 180 kyr and show similar ranges at all sites. Distinct glacial-interglacial differences are not observed, indicating that the source of the terrigenous matter or its underlying transport mechanism did not change. This is an interesting result, since records of %Siliciclastics, %Terrigen, and lithogenous element concentrations are characterized by significant variations on the glacial-interglacial level. Al/Ti ratios varied between 24–33 (mol mol^{-1}), with short-lived increases ($\sim$3) at the end of stage 4, and Terminations I and II. Average core Al/Ti values ($\sim$29.5 $\pm$ 3; Table 4), as well as surface sediment

CPD
8, 6135–6198, 2012

values from Shirshov Ridge (29.4 ± 4) and from the eastern Kamchatka continental margin (32.1 ± 3) (unpublished data) are almost identical, indicating that past and modern sources of terrigenous matter are identical. These values compare to Al/Ti ratios reported for Paleozoic (~ 29) and Mesozoic/Cenozoic shales (~ 32) from the Russian Platform (Ronov and Migdisov, 1971), but also with average values for sediment and continental crust (~ 28; McLennan, 1995; Taylor and McLennan, 1995), river particulate and mud (~ 30; McLennan, 1995), pelagic clay (~ 32; McLennan, 1995), as well as the range reported for loess deposits (~ 26–31; Taylor et al., 1983; Pye, 1987; McLennan, 1995). Values are clearly lower than that of the North American shale composite (~ 38; Gromet et al., 1984), but higher than Al/Ti ratios of oceanic tholeiitic basalt (~ 17; Engel et al., 1965) and surface samples from St. George Basin, SE Bering Sea (~ 24; Gardner et al., 1980). Nürnberg and Tiedemann (2004) reported a different range for sediments from the central Okhotsk Sea (~ 24–45).

The overall variability of Fe/Al ratios was between 0.20–0.34 (mol mol^{-1}) (Table 4). This range is in agreement with results from the central Okhotsk Sea (Nürnberg and Tiedemann, 2004). In contrast to Al/Ti, Fe/Al ratios along the core transect become increasingly higher towards the southernmost site since stage 3, with differences of up to ~ 0.06. A similar range (0.22–0.39) and meridional trend are observed in surface sediment samples from Shirshov Ridge (unpublished data). At the end of both glacial terminations short-lived decreases (~ 0.04) are found. Our Fe/Al ratios compare to those reported for the North American shale composite and average mud (~ 0.24; Gromet et al., 1984; McLennan, 1995), Mesozoic/Cenozoic (~ 0.26) and Paleozoic (~ 0.28) Russian Platform shales (Ronov and Migdisov, 1971), average values for river particulate (~ 0.25) and sediment (~ 0.27) (McLennan, 1995). Oceanic tholeiitic basalt (~ 0.28; Engel et al., 1965) and surface samples from St. George Basin (~ 0.28; Gardner et al., 1980) also apply to the overall range. The value for bulk continental crust is higher (~ 0.41; Taylor and McLennan, 1995), while loess deposits show a lower range between ~ 0.17–0.25 (Taylor et al., 1983; Pye, 1987; McLennan, 1995). From these results we conclude that sediments from Shirshov Ridge represent a mixture of

CPD
8, 6135–6198, 2012

geochemical signatures from aeolian sediments (loess) and continental sources that are supposedly not influenced by North American shales. The continental influence might successively decrease with increasing distance from the coast along the core transect.

4.2.3 Transport mechanism and source area

Possible mechanisms of terrigenous matter transport encompass fluvial and aeolian supply, as well as sea-ice rafting. Major rivers entering the Bering Sea are the Yukon and Anadyr rivers, which are situated at rather long distances from Shirshov Ridge (cf. Fig. 1). Given that further minor rivers in the surrounding of the Bering Sea are rare, we consider particulate material transport by rivers insignificant. Wind transported aerosols present in N Pacific sediments are restricted to the vicinity of their respective source area, which in our case are most likely situated in NE Siberia. Model results of global desert dust deposition show fluxes of 0.5–1.0 $g\,m^{-2}\,yr^{-1}$ for the Bering Sea (Mahowald et al., 2005), which implies that today aeolian input is negligible. This might, of course, have been different during past cold intervals as indicated by higher lithogenous element concentrations. Accordingly, we suggest that sea-ice rafting is and has been the prevailing transport agent of terrigenous matter at our sites. For the Arctic, Nürnberg et al. (1994) reported on sediments entrained in sea-ice to be generally fine grained (clayey silts, silty clays) and mainly composed of quartz, clay minerals and diatom flora. Sediments from the central Okhotsk Sea, which are also assumed to originate from sea-ice rafting are described as mainly clay and silt-sized siliciclastics (> 65 % siliciclastics) featuring dropstones (3–5 cm), and various lithogenic components (mainly quartz, rock fragments, mica, and dark minerals), with regionally different IRD composition (Nürnberg and Tiedemann, 2004; Nürnberg et al., 2011), which is comparable to that of our sediment cores. Since dropstones are rather uncommon in our cores, which, if present, appear as well rounded pebbles, we favor a beach deposit origin and tidal pumping, suspension freezing and beach-ice formation to be responsible for the entrainment of terrigenous matter into newly formed sea-ice.

CPD
8, 6135–6198, 2012

We favor sea-ice over iceberg transport due to the dominance of silt- and clay-sized terrigenous material, the absence of large dropstones, low variability in >63 µm, and the fact, that today no marine-terminating glaciers exist in the Bering Sea realm. Kaufman et al. (1996) suggested that the most recent major ice advance in SW Alaska occurred between ~90–75 ka BP. For stage 3 the proposed Kamchatka-Koryak Ice Sheet with marine-terminating ice margins (Bigg et al., 2008) was disproved (Nürnberg et al., 2011). Our cores lack evidence for iceberg discharge at ~40 ka BP (Bigg et al., 2008), therefore not supporting the suggested iceberg migration paths. For the LGM, the presence of the Beringian Ice Sheet (e.g. Grosswald and Hughes, 2002) has also been disproved (e.g. Brigham-Grette et al., 2001, 2003; Karhu et al., 2001), and Kamchatkan climate seems to have been too arid for the development of large continental ice sheets during that time (Barr and Clark, 2011).

Lisitzin (2002) identified mineralogical provinces for western Bering Sea surface sediments together with their possible migration paths and proposed that coarse silts and the larger grain-size fractions (pebbles, gravel, boulder) are controlled by sea-ice, sharing the same provinces and transport pathways. Accordingly, the Koryak Coast, Olyutorskii Bay, and northern Kamchatka provinces (cf. Fig. 1) likely are potential source areas for the ice rafted material in our sediments. Anadyr Bay, where modern seasonal sea-ice formation begins during fall, is as well taken into consideration. The K/Ti ratio is assumed to reflect temporal changes in sediment sources weathered from acidic (more K) and basaltic (more Ti) source rocks (Richter et al., 2006). Relatively increased K/Ti ratios are observed at times of enhanced terrigenous matter supply. If sea-ice rafting is the main driver of these changes, the geochemical source of the terrigenous matter (and consequently the ice-rafted material) would be characterized as being relatively increased in K. Of the considered provinces only Anadyr Bay is reported to contain acidic index rocks (Lisitzin, 2002), although geochemical data do not exist to clearly identify it as the proposed source area. However, this assumption is supported by the finding that interannual variability in Bering Sea ice cover is controlled by wind-driven

CPD
8, 6135–6198, 2012

ice mass advection, which clearly is southwestward from Anadyr Bay (Zhang et al., 2010).

4.3 Environmental changes during the last 180 kyr

4.3.1 Glacial situation

Cold intervals of the last 180 kyr seem to have been subject to strongly reduced, but maintained primary productivity at our sites. At the same time, our records indicate high input of terrigenous matter, which is in agreement with records from the Okhotsk Sea (Nürnberg and Tiedemann, 2004; Nürnberg et al., 2011). Although regionally different, low glacial export production characterizes the whole N Pacific during the last 800 kyr (for a review see Kienast et al., 2004). Nürnberg et al. (2011) argued for extreme glacial ice conditions in the Okhotsk Sea during stage 6 with a potentially perennial ice coverage. From our results, we can not infer that conditions during stage 6 were significantly different from those during later cold intervals. Glacial conditions in the Okhotsk Sea are supposed to be similar to the modern winter situation of a strong Siberian High and a weak Aleutian Low, thereby resulting in strong offshore, northerly winds (Nürnberg and Tiedemann, 2004; Nürnberg et al., 2011). This situation might as well apply to the Bering Sea and would have resulted in enhanced sea-ice formation during a generally colder climate, thereby explaining the higher LSR and terrigenous inputs. At Bowers Ridge, at least for stages 3 and 2, colder subsurface temperatures are supported by low total numbers of planktonic foraminifera, dominated by polar species *Neogloboquadrina pachyderma* (sin.) and reduced/absent numbers of subpolar species *Globigerina bulloides* (Gorbarenko et al., 2005). A spatially extended sea-ice coverage fostered by a shortened summer season might have resulted in enhanced upper-ocean stratification and reduced nutrient supply to the surface ocean. Since primary productivity is limited by temperature and nutrient availability, the prolonged sea-ice season during colder intervals would have consequently led to the reduction in marine productivity observed at our sites. This should be reflected by stronger nutrient utilization,

CPD
8, 6135–6198, 2012

and indeed, bulk sediment and diatom-bound nitrogen isotope ratios (δ^{15}N) recorded at Bowers Ridge (Brunelle et al., 2007) show higher glacial than interglacial values (Fig. 9), thereby confirming earlier assumptions of suppressed vertical mixing in the glacial Bering Sea (Nakatsuka et al., 1995).

In HNLC regions primary production is limited by the availability of Fe (Fe-fertilization). During glacials increasing primary production was observed in the HNLC region of the equatorial Pacific, implying a link to Fe delivery (Murray et al., 2012). Although the western Bering Sea basin is considered as HNLC (Tyrrell et al., 2005), we found high glacial [Fe] values despite low marine productivity. Accordingly, we neglect Fe-fertilization as the limiting factor of primary production on glacial-interglacial timescales in the western Bering Sea. Support for an extended sea-ice coverage in the Bering Sea during glacial periods comes from diatom and radiolarian assemblages (Katsuki and Takahashi, 2005; Tanaka and Takahashi, 2005).

It has been speculated, that the net-inflow of Alaskan Stream waters into the Bering Sea was reduced at times when the Bering Strait and/or other Aleutian passes, like Unimak Pass, were closed due to lower glacial sea-level, thereby affecting Beringian climate (Pushkar et al., 1999; Tanaka and Takahashi, 2005). During stage 2, a strengthened Subarctic Front could have additionally led to a reduced inflow of warmer and nutrient-enriched Pacific surface waters (Gorbarenko et al., 2005). In consequence, nutrient supply to the Bering Sea should have been further reduced and have resulted in stronger nutrient utilization. The relative sea-level (RSL) reconstruction of Waelbroek et al. (2002) implies that the Bering Strait was closed during stage 6, as well as in between stages 4 and 2 (Fig. 9), while its last major re-opening occurred at 12–11 ka BP (Keigwin et al., 2006). RSL changes in the Bering Strait are predominantly controlled by eustatic changes and suggested to considerably influence deep convection in the N Atlantic (Hu et al., 2010). At Bowers Ridge δ^{15}N values are highest during stages 3 and 2 (Fig. 9), supporting an influence of RSL on upper-ocean stratification and, hence, nitrate utilization in the Bering Sea.

CPD
8, 6135–6198, 2012

The low glacial $CaCO_3$ concentrations and abundances of oxic benthic foraminifera species point towards the presence of corrosive bottom waters as a result of organic matter degradation under oxic bottom water conditions (Kim et al., 2011). This implies that either O_2-rich intermediate water masses were formed in the Bering Sea, or flew in from the Pacific side. Sea-ice formation in the Bering Sea due to brine rejection results in denser, O_2-rich surface waters (e.g. Niebauer et al., 1999), and thus might have maintained the production and ventilation of intermediate water. Rella et al. (2012) reported on benthic $\delta^{18}O$ excursions in sediments from the northern slope, which implies that the Bering Sea was a source of intermediate water during past stadial episodes, which is supported by microfossil assemblages (Ohkushi et al., 2003). However, as the modern origin of NPIW lies in the Okhotsk Sea (Yasuda, 1997) and during glacial stages a closed Bering Strait prevented inflow of surface waters from the Arctic Ocean (Takahashi, 1998, 1999), inflow from the N Pacific can not be ruled out.

4.3.2 Deglacial situation

During Termination I high marine productivity but low terrigenous input is observed during the B/A and PB warm phases, whereas the opposite situation occurred during the H1 and YD cold phases. Remarkably, SST records from our sites mirror the deglacial SST evolution recorded in the N Atlantic, supporting quasi-synchronity of Northern Hemisphere climate changes (Max et al., 2012). The early deglacial phase starts with increasing [C/N]a ratios, LSR, and TOC just after the LGM at ~17 ka BP. This is explained by higher input of terrestrial organic matter derived from flooded shelf areas in the course of sea-level rise and was previously suggested for the Okhotsk and Bering seas (Ternois et al., 2001; Seki et al., 2003; Khim et al., 2010). Notably, at the northern slope similar changes were reported to have occurred ~2 kyr earlier (Khim et al., 2010). This timelag for increased terrigenous carbon input suggests that both locations were supplied from different sources, which for the northern slope might be related to terrestrial runoff from Yukon River denitrifying the eastern continental shelf.

CPD
8, 6135–6198, 2012

Our records indicate enhanced sea-ice rafting during H1 and the YD, which for our sites is supported by the presence of the sea-ice-related IP_{25} biomarker (Max et al., 2012) and by increasing abundances of the sea-ice-related diatom genus *Nitzschia* at Umnak Plateau (Cook et al., 2005). Like during previous cold intervals, primary production was restricted by lowered temperature. A sudden decrease in bulk sedimentary and diatom-bound $\delta^{15}N$ (Fig. 9) point to decreased nitrate utilization (Brunelle et al., 2007, 2010) as a result of fresh nutrient supply due to stonger vertical mixing. Support for intensified mixing and/or overturning during H1 comes from reduced ventilation ages in the N Pacific realm (Ohkushi et al., 2004; Sarnthein et al., 2007; Sagawa and Ikehara, 2008; Okazaki et al., 2010), benthic $\delta^{18}O$ (Rella et al., 2012), as well as modeling studies (e.g. Okazaki et al., 2010; Chikamoto et al., 2012; Menviel et al., 2012), and was related to the potential disappearance of the halocline. Subsequent to H1, increasing insolation and sea-level rise amplified the surface ocean warming, which might have led to more dynamic ice conditions, northward propagating ice margins, and a prolonged sea-ice-free summer season. Indeed, rising SST and beginning coccolithophorid production are inferred from first detectable concentrations of alkenones (Caissie et al., 2010; Max et al., 2012).

The onset of the B/A, and to a lesser degree also the PB phase, is characterized by increasing values in all productivity proxies, while LSR and most proxies for terrigenous supply decline. Records of > 63 µm instead show a peak, which we attribute to the sudden release of IRD from melting sea-ice. Similar observations regarding changes in marine productivity have previously been reported for the Bering Sea (Gorbarenko, 1996; Cook et al., 2005; Gorbarenko et al., 2005; Okazaki et al., 2005; Khim et al., 2010) and other parts of the N Pacific (Keigwin and Jones, 1990; Keigwin et al., 1992; Gorbarenko, 1996; Keigwin, 1998; Crusius et al., 2004; McKay et al., 2004; Okazaki et al., 2005; Gebhardt et al., 2008). Rising summer SSTs (stronger seasonal contrasts) amplified sea-ice melting and resulted in strengthened mixed layer stratification (Riethdorf et al., 2012). Enhanced surface freshening due to melting sea-ice is supported by higher abundances of radiolarian species *Rhizoplegma boreale* (Kim et al., 2011), as

CPD
8, 6135–6198, 2012

well as brackish diatom species *Paralia sulcata* (Gorbarenko et al., 2005). Evidence for reduced ventilation with respect to H1 comes from higher ventilation ages found in the N Pacific (Adkins and Boyle, 1997; Ahagon et al., 2003; Ohkushi et al., 2004; Sagawa and Ikehara, 2008; Okazaki et al., 2010). A maximum in δ^{15}N values (Fig. 9) implies increased nitrate utilization or even denitrification of seawater nitrate in response to stronger stratification (Brunelle et al., 2007, 2010; Khim et al., 2010). It might further be speculated, that the increase in marine productivity associated with reduced sea-ice formation resulted in organic matter supply exceeding its degradation at the seafloor. In consequence, bottom water conditions might have become dysoxic or anoxic, impeding benthonic life and favouring laminae formation. This notion is in agreement with the formation of dysoxic or laminated sediments observed at oxygen minimum zone (OMZ) depths in the N Pacific and Bering Sea during the B/A and PB (van Geen et al., 2003; Cook, 2006, and references therein) and most probably was related to an intensification of the OMZ (Zheng et al., 2000). At the same time the respired carbon pool was obviously removed from the deep basin, which resulted in enhanced carbonate preservation due to a deepened lysocline, and to an increase in atmospheric CO_2 (e.g. Galbraith et al., 2007).

Our records show that at sites 85KL and 101KL the deglacial development during Termination II does not resemble that of Termination I. Most notably, extremely high amounts of coarse material are recorded at the end of Termination II, which is not observed previously or later at any site. At the same time excursions towards lower Fe/Al but higher Al/Ti ratios were recorded, indicating a slightly different geochemical composition of the sediments. We attribute these results to the sudden release of IRD in response to strong melting of a potentially perennial ice coverage as suggested for the Okhotsk Sea (Nürnberg et al., 2011). Also, records of benthic δ^{18}O do not follow the LR04 stack, which is indicative of a strong regional effect on the δ^{18}O signal, e.g. by melting of continental ice sheets in the Bering Sea realm.

CPD
8, 6135–6198, 2012

4.3.3 Interglacial situation

In contrast to the situation during cold intervals, interglacials, as well as warm stages 5.3 and 5.1 are characterized by increased marine productivity and decreased terrigenous matter supply. Meridional gradients are observed along the core transect with reduced sea-ice influence favouring marine productivity towards the southernmost site. Especially during interglacials results for Site 77KL better compare to those reported for Bowers Ridge, whereas sites 85KL and 101KL resemble records from the northern slope and the central Okhotsk Sea. Marine productivity as reflected by opal concentrations was higher during stage 5.5 than during the Holocene. Interglacial $CaCO_3$ concentrations remained at or close to glacial values implying a similar bottom water calcite saturation state with limited carbonate preservation. Increased marine productivity most probably resulted from warmer temperatures and reduced sea-ice formation during a prolonged summer season (stronger seasonal contrasts). However, our records imply a reduction of only ∼30–40 % in terrigenous matter supply. Overall, records of XRF Si/Al log-ratios are in phase with mean summer insolation at 65° N (July–September; calculated after Laskar, 2004; Fig. 9), showing maxima during stages 5.5, 5.3, 5.1, and 1. This implies a dominant insolation forcing for environmental changes in the Bering Sea. At Bowers Ridge, δ^{15}N values are lowest during interglacials (Brunelle et al., 2007, 2010) and they also remain low during most of stage 5 (Fig. 9), indicative of reduced nitrate utilization as a consequence of enhanced vertical mixing and allochthonous nutrient supply. This situation might have been fostered by an open Bering Strait and Unimak Pass, allowing for enhanced inflow of relatively warmer and nutrient-enriched water masses from the Alaskan Stream. Reduced sea-ice formation, but enhanced nutrient supply and vertical mixing as a result of a strengthened Alaskan Stream and Bering Slope Current during higher sea-level has been proposed before (Gorbarenko et al., 2005; Okazaki et al., 2005; Kim et al., 2011). Accordingly, we consider additional sea-level forcing to explain the recorded environmental changes.

CPD
8, 6135–6198, 2012

4.3.4 Interstadial situation

High-resolution core logging resulted in the detection of short-lived maxima in our color b* and XRF Ca/Ti log-ratio records during stages 6 to 3. Notably, they occur together with maxima in > 63 µm. Most peaks were detected in cores 85KL and 101KL within which they are characterized by only 1–3 cm sediment thickness corresponding to a duration of ~ 100–300 yr. These changes in sediment composition seem to be related to D-O events (interstadials) registered in the NGRIP ice core. The most prominent events correspond to D-O events 7, 8, 12, 17–21, and 24 (Fig. 5), but events off the NGRIP record are found. We consider them as brief intervals of enhanced marine productivity, sudden sea-ice melt and subsequent release of IRD, and a higher bottom water calcite saturation state. However, due to our stratigraphic approach, which relies on the NGRIP record, we can neither argue for nor against an in-phase evolution between abrupt climate changes recorded in Greenland ice and western Bering Sea sediments. Sediment records from Bowers Ridge (Gorbarenko et al., 2005, 2010), the northern slope (Kim et al., 2011; Rella et al., 2012), as well as the NE Pacific (Behl and Kennett, 1996; Hendy and Kennett, 2000; Ortiz et al., 2004) also implied millennial-scale climate changes connected to N Atlantic D-O events, especially during stage 3. Similar features were detected in stalagmites from China (Wang et al., 2001, 2008), which indicates a Northern Hemisphere-wide acting atmospheric coupling that is related to the intensity of the East Asian Monsoon. Kennett and Ingram (1995) proposed that such an atmospheric coupling mechanism directly affected the ventilation of NPIW. Accordingly, interstadials seem to have been characterized by weak ventilation of NPIW in combination with increased marine productivity (Behl and Kennett, 1996; Hendy and Kennett, 2000; Kim et al., 2011) and warmer SSTs (Gorbarenko et al., 2005). Recently, Kim et al. (2011) reported on D-O event-related brief episodes of high bulk $\delta^{15}N$ values at the northern slope, implying increased nitrate utilization/denitrification. These results to a lesser degree reflect conditions inferred for the B/A warm phase and thus might point to the release of deep-sequestered CO_2 during interstadials.

CPD
8, 6135–6198, 2012

5 Summary and conclusions

From our results we proposed scenarios for environmental change in the Bering Sea during glacial, deglacial, and interglacial times which compare to those suggested for the Okhotsk Sea. During the last 180 kyr, the Bering Sea paleoenvironment was characterized by closely interacting processes controlling marine productivity and terrigenous matter supply. External forcing is attributed to Northern Hemisphere summer insolation and sea-level changes controlling atmospheric circulation patterns, sea-ice dynamics and upper-ocean stratification. Marine productivity, dominated by diatoms, remained low during cold intervals (stages 6, 5.4, 5.2, 4, and 2) when the Bering Strait was closed and summer insolation was weak. Significant increases occured during warm intervals (stages 5.5, 5.3, 5.1, and 1), when insolation was high and the Bering Strait was open. Sediment composition is dominated by terrigenous, siliciclastic material mainly bound to the fine fractions. Terrigenous matter supply was generally high with reductions of up to ~30–40 % during interglacials. Changes in terrigenous matter supply and marine productivity occurred synchronously with anticorrelated proxy behaviour. Meridional gradients were found along our core transect, suggesting stronger sea-ice influence and, hence, restricted marine productivity towards the northernmost site. Sea-ice rafting is considered as the predominant transport agent for terrigenous matter, limiting marine productivity during cold intervals. Sedimentary geochemical signatures are a mixture of aeolian and continental sources, indicating that Shirshov Ridge sediments most likely originate from sea-ice formation in Anadyr Bay. Especially for the last glacial termination our records support the notion of an atmospheric, Northern Hemisphere-wide acting climate coupling. The situation during the H1 and YD cold phases compared to that of cold intervals with enhanced sea-ice rafting limiting marine productivity during a shortened summer season (weak seasonal contrasts). In contrast, the B/A and PB warm phases were characterized by enhanced marine productivity as a result of a prolonged summer season and reduced sea-ice influence (strong seasonal contrasts). At the same time, reduced ventilation of intermediate waters is

CPD
8, 6135–6198, 2012

in accordance with higher nitrate utilization and better $CaCO_3$ preservation indicative of a release of deep-sequestered CO_2 to the atmosphere. Moreover, we found evidence for abrupt environmental changes that are related to interstadials recorded in the NGRIP ice core and reflect the situation proposed for the B/A.

Appendix A

Age models

Age-depth points for cores SO201-2-77KL, −85KL, and −101KL are given in Tables A1, A2, and A3, respectively.

Acknowledgements. This study resulted from the German-Russian joint research project KALMAR, funded by the German Ministry of Education and Research (BMBF), grant nos. 03G0672A and B. We thank the captain and crew of R/V *Sonne cruise* SO201-KALMAR Leg 2 for their professional support in recovering high-quality cores. Technical support and laboratory assistance came from B. Domeyer, N. Gehre, L. Haxhiaj, P. Appel, and J. Heinze and is gratefully acknowledged. E. Maier (AWI-Bremerhaven) conducted additional opal measurements for core 77KL. A. Matul (Shirshov Institute of Oceanology, Moscow) provided additional benthic foraminiferal tests to improve oxygen isotope stratigraphy for cores 85KL and 101KL. The data are available via the PANGAEA Data Publisher for Earth & Environmental Science (http://doi.pangaea.de/10.1594/PANGAEA.786307).

The service charges for this open access publication have been covered by a Research Centre of the Helmholtz Association.

CPD
8, 6135–6198, 2012

References

Adkins, J. F. and Boyle, E. A.: Changing atmospheric $\Delta^{14}C$ and the record of deep water paleoventilation ages, Paleoceanography, 12, 337–344. 1997.

Ahagon, N., Ohkushi, K., Uchida, M., and Mishima, T.: Mid-depth circulation in the northwest Pacific during the last deglaciation: evidence from foraminiferal radiocarbon ages, Geophys. Res. Lett., 30, 2097, doi:10.1029/2003GL018287, 2003.

Arzhanova, N. V., Zubarevich, V. L., and Sapozhnikov, V. V.: Seasonal variability of nutrient stocks in the euphotic zone and assessment of primary production in the Bering Sea, in: Complex studies of the Bering Sea ecosystem, edited by: Kotenev, B. N. and Sapozhnikov, V. V., VNIRO, Moscow, 162–179, 1995.

Bareille, G., Grousset, F. E., Labracherie, M., Labeyrie, L. D., and Petit, J.-R.: Origin of detrital fluxes in the southeast Indian Ocean during the last climatic cycles, Paleoceanography, 9, 799–819, 1994.

Barr, I. D. and Clark, C. D.: Glaciers and climate in Pacific Far NE Russia during the Last Glacial Maximum, J. Quaternary Sci., 26, 227–237, 2011.

Behl, R. J. and Kennett, J. P.: Brief interstadial events in the Santa Barbara Basin, NE Pacific, during the past 60 kyr, Nature, 379, 243–246, 1996.

Bigg, G. R., Clark, C. D., and Hughes, A. L. C.: A last glacial ice sheet on the Pacific Russian coast and catastrophic change arising from coupled ice-volcanic interaction, Earth Planet. Sc. Lett., 265, 559–570, 2008.

Blockley, S. P. E., Lane, C. S., Hardiman, M., Rasmussen, S. O., Seierstad, I. K., Steffensen, J. P., Svensson, A., Lotter, A. F., Turney, C. S. M., Ramsey, C. B., and INTIMATE members: Synchronisation of palaeoenvironmental records over the last 60,000 years, and an extended INTIMATE event stratigraphy to 48,000 b2k, Quaternary Sci. Rev., 36, 2–10, 2012.

Boyle, E. A.: Chemical accumulation variations under the Peru current during the past 130,000 years, J. Geophys. Res., 88, 7667–7680, 1983.

Brigham-Grette, J., Hopkins, D. M., Ivanov, V. F., Basilyan, E. B., Benson, S. L., Heiser, P. A., and Pushkar, V. S.: Last Interglacial (isotope stage 5) glacial and sea-level history of coastal Chukotka Peninsula and St. Lawrence Island, Western Beringia, Quaternary Sci. Rev., 20, 419–436, 2001.

CPD
8, 6135–6198, 2012

Brigham-Grette, J., Gualtieri, L. M., Glushkova, O. Y., Hamilton, T. D., Mostoller, D., and Kotov, A.: Chlorine-35 and ^{14}C chronology support a limited last glacial maximum across central Chukotka, northeastern Siberia, and no Beringian ice sheet, Quaternary Res., 59, 386–398, 2003.

Broecker, W. S. and Peng, T.-H.: The role of $CaCO_3$ compensation in the glacial to interglacial atmospheric CO_2 change, Global Biogeochem. Cy., 1, 15–29, 1987.

Brunelle, B. G., Sigman, D. M., Cook, M. S., Keigwin, L. D., Haug, G. H., Plessen, B., Schettler, G., and Jaccard, S. L.: Evidence from diatom-bound nitrogen isotopes for subarctic Pacific stratification during the last ice age and a link to North Pacific denitrification changes, Paleoceanography, 22, PA1215, doi:10.1029/2005PA001205, 2007.

Brunelle, B. G., Sigman, D. M., Jaccard, S. L., Keigwin, L. D., Plessen, B., Schettler, G., Cook, M. S., and Haug, G. H.: Glacial/interglacial changes in nutrient supply and stratification in the western subarctic North Pacific since the penultimate glacial maximum, Quaternary Sci. Rev., 29, 2579–2590, 2010.

Burov, B. V., Nourgaliev, D. K., and Iassonov, P. G.: Paleomagnetic analysis, Kazan University Press, Kazan, 167 pp., 1986 (in Russian).

Caissie, B. E., Brigham-Grette, J., Lawrence, K. T., Herbert, T. D., and Cook, M. S.: Last Glacial Maximum to Holocene sea surface conditions at Umnak Plateau, Bering Sea, as inferred from diatom, alkenone, and stable isotope records, Paleoceanography, 25, PA1206, doi:10.1029/2008PA001671, 2010.

Calvert, S. E. and Fontugne, M. R.: On the late Pleistocene-Holocene sapropel record of climatic and oceanographic variability in the eastern Mediterranean, Paleoceanography, 16, 78–94, 2001.

Channell, J. E. T., Xuan, C., and Hodell, D. A.: Stacking paleointensity and oxygen isotope data for the last 1.5 Myr (PISO-1500), Earth Planet. Sc. Lett., 283, 14–23, 2009.

Chen, C.-T. A.: Shelf-vs. dissolution-generated alkalinity above the chemical lysocline, Deep-Sea Res. Pt. II, 49, 5365–5375, 2002.

Chikamoto, M. O., Menviel, L., Abe-Ouchi, A., Ohgaito, R., Timmermann, A., Okazaki, Y., Harada, N., Oka, A., and Mouchet, A.: Variability in North Pacific intermediate and deep water ventilation during Heinrich events in two coupled climate models, Deep-Sea Res. Pt. II, 61–64, 114–126, 2012.

CPD
8, 6135–6198, 2012

Cook, M. S.: The paleoceanography of the Bering Sea during the last glacial cycle, Ph.D. thesis, Massachusetts Institute of Technology, Woods Hole Oceanographic Institution, Massachusetts Institute of Technology, 126 pp., 2006.
Cook, M. S., Keigwin, L. D., and Sancetta, C. A.: The deglacial history of surface and intermediate water of the Bering Sea, Deep-Sea Res. Pt. II, 52, 2163–2173, 2005.
Crusius, J., Pedersen, T. F., Kienast, S., Keigwin, L., and Labeyrie, L.: Influence of northwest Pacific productivity on North Pacific Intermediate Water oxygen concentrations during the Bölling-Alleröd interval (14.7–12.9 ka), Geology, 32, 633–636, 2004.
Dehairs, F., Stroobants, N., and Goeyens, L.: Suspended barite as a tracer of biological activity in the Southern Ocean, Mar. Chem., 35, 399–410, 1991.
De La Rocha, C. L.: The biological pump, in: Treatise on Geochemistry, vol. 6, edited by: Elderfield, H., Elsevier, Amsterdam, 83–111, 2007.
DeMaster, D.: The supply and accumulation of silica in the marine environment, Geochim. Cosmochim. Ac., 45, 1715–1732, 1981.
Duce, R. A. and Tindale, N. W.: Atmospheric transport of iron and its deposition in the ocean, Limnol. Oceanogr., 36, 1715–1726, 1991.
Dullo, W.-C., Baranov, B., and van den Bogaard, C. (Eds.): FS *Sonne* Fahrtbericht/Cruise Report SO201–2 KALMAR, Busan/Korea–Tomakomai/Japan, 30.08.–08.10.2009, IFM-GEOMAR Report 35, Leibniz Institute of Marine Sciences, Kiel, 233 pp., 2009.
Dymond, J. and Collier, R.: Particulate barium fluxes and their relationships to biological productivity, Deep-Sea Res. Pt. II, 43, 1283–1308, 1996.
Dymond, J., Suess, E., and Lyle, M.: Barium in deep-sea sediment: a geochemical proxy for paleoproductivity, Paleoceanography, 7, 163–181, 1992.
Emile-Geay, J., Cane, M. A., Naik, N., Seager, R., Clement, A. C., and van Geen, A.: Warren revisited: atmospheric freshwater fluxes and "Why is no deep water formed in the North Pacific", J. Geophys. Res., 108, 3178, doi:10.1029/2001JC001058, 2003.
Engel, A. E. J., Engel, C. G., and Havens, R. G.: Chemical characteristics of oceanic basalts and the upper Miocene, Geol. Soc. Am. Bull., 76, 719–734, 1965.
Enkin, R. J., Baker, J., Nourgaliev, D., Iassonov, P., and Hamilton, T. S.: Magnetic hysteresis parameters and Day plot analysis to characterize diagenetic alteration in gas hydrate-bearing sediments, J. Geophys. Res., 112, B06S90, doi:10.1029/2006JB004638, 2007.
Eppley, R. W. and Peterson, B. J.: Particulate organic matter flux and planktonic new production in the deep ocean, Nature, 282, 677–680, 1979.

CPD
8, 6135–6198, 2012

Feely, R. A., Sabine, C. L., Lee, K., Millero, F. J., Lamb, M. F., Greeley, D., Bullister, J. L., Key, R. M., Peng, T.-H., Kozyr, A., Ono, T., and Wong, C. S.: In situ calcium carbonate dissolution in the Pacific Ocean, Global Biogeochem. Cy., 16, 1144, doi:10.1029/2002GB001866, 2002.

Francois, R., Honjo, S., Manganini, S. J., Ravizza, G. E.: Biogenic barium fluxes to the deep sea: implications for paleoproductivity reconstruction, Global Biogeochem. Cy., 9, 289–303, 1995.

Galbraith, E. D., Jaccard, S. L., Pedersen, T. F., Sigman, D. M., Haug, G. H., Cook, M., Southon, J. R., and Francois, R.: Carbon dioxide release from the North Pacific abyss during the last deglaciation, Nature, 449, 890–893, 2007.

Galbraith, E. D., Kienast, M., Jaccard, S. L., Pedersen, T. F., Brunelle, B. G., Sigman, D. M., and Kiefer, T.: Consistent relationship between global climate and surface nitrate utilization in the western subarctic Pacific throughout the last 500 ka, Paleoceanography, 23, PA2212, doi:10.1029/2007PA001518, 2008.

Ganeshram, R. S., Calvert, S. E., Pedersen, T. F., and Cowie, G. L.: Factors controlling the burial of organic carbon in laminated and bioturbated sediments off NW Mexico: implications for hydrocarbon preservation, Geochim. Cosmochim. Ac., 63, 1723–1734, 1999.

Gardner, J. V., Dean, W. E., and Vallier, T. L.: Sedimentology and geochemistry of surface sediments, outer continental shelf, southern Bering Sea, Mar. Geol., 35, 299–329, 1980.

Gebhardt, H., Sarnthein, M., Grootes, P. M., Kiefer, T., Kühn, H., Schmieder, F., and Röhl, U.: Paleonutrient and productivity records from the subarctic North Pacific for Pleistocene glacial terminations I to V, Paleoceanography, 23, PA4212, doi:10.1029/2007PA001513, 2008.

Gingele, F., Zabel, M., Kasten, S., Bonn, W. J., and Nürnberg, C. C.: Biogenic barium as a proxy for paleoproductivity: methods and limitations of application, in: Use of Proxies in Paleoceanography, Examples from the South Atlantic, edited by: Fischer, G. and Wefer, G., Springer, Berlin, 345–364, 1999.

Goñi, M. A., Ruttenberg, K. C., and Eglinton, T. I.: A reassessment of the sources and importance of land-derived organic matter in surface sediments from the Gulf of Mexico, Geochim. Cosmochim. Ac., 62, 3055–3075, 1998.

Gorbarenko, S. A.: Stable isotope and lithologic evidence of late-glacial and Holocene oceanography of the northwestern Pacific and its marginal seas, Quaternary Res., 46, 230–250, 1996.

CPD
8, 6135–6198, 2012

Gorbarenko, S. A., Khusid, T. A., Basov, I. A., Oba, T., Southon, J. R., and Koizumi, I.: Glacial Holocene environment of the southeastern Okhotsk Sea: evidence from geochemical and paleontological data, Palaeogeogr. Palaeocl., 177, 237–263, 2002a.

Gorbarenko, S. A., Nürnberg, D., Derkachev, A. N., Astakhov, A. S., Southon, J. R., and Kaiser, A.: Magnetostratigraphy and tephrochronology of the Upper Quaternary sediments in the Okhotsk Sea: implication of terrigenous, volcanogenic and biogenic matter supply, Mar. Geol., 183, 107–129, 2002b.

Gorbarenko, S. A., Basov, I. A., Chekhovskaya, M. P., Southon, J., Khusid, T. A., and Artemova, A. V.: Orbital and millenium scale environmental changes in the southern Bering Sea during the last glacial-Holocene: geochemical and paleontological evidence, Deep-Sea Res. Pt. II, 52, 2174–2185, 2005.

Gorbarenko, S. A., Wang, P., Wang, R., and Cheng, X.: Orbital and suborbital environmental changes in the southern Bering Sea during the last 50 kyr, Palaeogeogr. Palaeocl., 286, 97–106, 2010.

Gromet, L. P., Dymek, R. F., Haskin, L. A., and Korotev, R. L.: The "North American shale composite": its compilation, major and trace element characteristics, Geochim. Cosmochim. Ac., 48, 2469–2482, 1984.

Grosswald, M. G. and Hughes, T. J.: The Russian component of an Arctic Ice Sheet during the Last Glacial Maximum, Quaternary Sci. Rev., 21, 121–146, 2002.

Hartnett, H. E., Keil, R. G., Hedges, J. I., and Devol, A. H.: Influence of oxygen exposure time on organic carbon preservation in continental margin sediments, Nature, 391, 572–574, 1998.

Haug, G. H., Sigman, D. M., Tiedemann, R., Pedersen, T. F., and Sarnthein, M.: Onset of permanent stratification in the subarctic Pacific Ocean, Nature, 401, 779–782, 1999.

Haug, G. H., Ganopolski, A., Sigman, D. M., Rosell-Mele, A., Swann, G. E. A., Tiedemann, R., Jaccard, S. L., Bollmann, J., Maslin, M. A., Leng, M. J., and Eglinton, G.: North Pacific seasonality and the glaciation of North America 2.7 million years ago, Nature, 433, 821–825, 2005.

Hedges, J. I., Clark, W. A., Quay, P. D., Richey, J. E., Devol, A. H., and de M. Santos, U.: Compositions and fluxes of particulate organic material in the Amazon River, Limnol. Oceanogr., 31, 717–738, 1986.

Hedges, J. I., Baldock, J. A., Gélinas, Y., Lee, C., Peterson, M., and Wakeham, S. G.: Evidence for non-selective preservation of organic matter in sinking marine particles, Nature, 409, 801–804, 2001.

CPD
8, 6135–6198, 2012

Hendy, I. L. and Kennett, J. P.: Dansgaard–Oeschger cycles and the California Current System: planktonic foraminiferal response to rapid climate change in Santa Barbara Basin, Ocean Drilling Program Hole 893A, Paleoceanography, 15, 30–42, 2000.

Honda, M. C., Imai, K., Nojiri, Y., Hoshi, F., Sugawara, T., and Kusakabe, M.: The biological pump in the northwestern North Pacific based on fluxes and major components of particulate matter obtained by sediment-trap experiments (1997–2000), Deep-Sea Res. Pt. II, 49, 5595–5625, 2002.

Hu, A., Meehl, G. A., Otto-Bliesner, B. L., Waelbroeck, C., Han, W., Loutre, M.-F., Lambeck, K., Mitrovica, J. X., and Rosenbloom, N.: Influence of Bering Strait flow and North Atlantic circulation on glacial sea-level changes, Nat. Geosci., 3, 118–121, 2010.

Itaki, T., Uchida, M., Kim, S., Shin, H.-S., Tada, R., and Khim, B.-K.: Late Pleistocene stratigraphy and palaeoceanographic implications in northern Bering Sea slope sediments: evidence from the radiolarian species *Cycladophora davisiana*, J. Quaternary Sci., 24, 856–865, 2009.

Jaccard, S. L., Haug, G. H., Sigman, D. M., Pedersen, T. F., Thierstein, H. R., and Röhl, U.: Glacial/interglacial changes in subarctic North Pacific stratification, Science, 308, 1003–1008, 2005.

Jaccard, S. L., Galbraith, E. D., Sigman, D. M., Haug, G. H., Francois, R., Pedersen, T. F., Dulski, P., and Thierstein, H. R.: Subarctic Pacific evidence for a glacial deepening of the oceanic respired carbon pool, Earth Planet. Sc. Lett., 277, 156–165, 2009.

Jaccard, S. L., Galbraith, E. D., Sigman, D. M., and Haug, G. H.: A pervasive link between Antarctic ice core and subarctic Pacific sediment records over the past 800 kyrs, Quaternary Sci. Rev., 29, 206–212, 2010.

Jansen, J. H. F., van der Gaast, S. J., Koster, B., and Vaars, A. J.: CORTEX, a shipboard XRF-scanner for element analyses in split sediment cores, Mar. Geol., 151, 143–153, 1998.

Karhu, J. A., Tschudi, S., Saarnisto, M., Kubik, P., and Schlüchter, C.: Constraints for the latest glacial advance on Wrangel Island, Arctic Ocean, from rock surface exposure dating, Global Planet. Change, 31, 447–451, 2001.

Katsuki, K. and Takahashi, K.: Diatoms as paleoenvironmental proxies for seasonal productivity, sea-ice and surface circulation in the Bering Sea during the late Quaternary, Deep-Sea Res. Pt. II, 52, 2110–2130, 2005.

Kaufman, D. S., Forman, S. L., Lea, P. D., and Wobus, C. W.: Age of pre-late-Wisconsin glacial-eastuarine sedimentation, Bristol Bay, Alaska, Quaternary Res., 45, 59–72, 1996.

CPD
8, 6135–6198, 2012

Keigwin, L. D.: Glacial-age hydrography of the far northwest Pacific Ocean, Paleoceanography, 13, 323–339, 1998.
Keigwin, L. D. and Jones, G. A.: Deglacial climatic oscillations in the Gulf of California, Paleoceanography, 5, 1009–1023, 1990.
Keigwin, L. D., Jones, G. A., and Froelich, P. N.: A 15,000 year paleoenvironmental record from Meiji Seamount, far northwestern Pacific, Earth Planet. Sc. Lett., 111, 425–440, 1992.
Keigwin, L. D., Donnelly, J. P., Cook, M. S., Driscoll, N. W., and Brigham-Grette, J.: Rapid sea-level rise and Holocene climate in the Chukchi Sea, Geology, 34, 861–864, doi:10.1130/G22712.1, 2006.
Kennett, J. P. and Ingram, B. L.: A 20,000-year record of ocean circulation and climate change from the Santa Barbara Basin, Nature, 377, 510–514, 1995.
Khim, B.-K., Kim, S., Uchida, M., and Itaki, T.: High organic carbon deposition in the northern margin of the Aleutian Basin (Bering Sea) before the last deglaciation, Ocean Sci. J., 45, 203–211, 2010.
Kienast, S. S., Hendy, I. L., Crusius, J., Pedersen, T. F., and Calvert, S.: Export production in the subarctic North Pacific over the last 800 kyrs: no evidence for iron fertilization?, J. Oceanogr., 60, 189–203, 2004.
Kim, S., Khim, B. K., Uchida, M., Itaki, T., and Tada, R.: Millennial-scale paleoceanographic events and implication for the intermediate-water ventilation in the northern slope area of the Bering Sea during the last 71 kyrs, Global Planet. Change, 79, 89–98, 2011.
Klump, J., Hebbeln, D., and Wefer, G.: The impact of sediment provenance on barium-based productivity estimates, Mar. Geol., 169, 259–271, 2000.
Laskar, J., Robutel, P., Joutel, F., Gastineau, M., Correia, A. C. M., and Levrard, B.: A long-term numerical solution for the insolation quantities of the Earth, Astron. Astrophys., 428, 261–285, doi:10.1051/0004-6361:20041335, 2004.
Latimer, J. C. and Filippelli, G. M.: Terrigenous input and paleoproductivity in the Southern Ocean, Paleoceanography, 16, 627–643, 2001.
Lisiecki, L. and Raymo, M.: A Pliocene-Pleistocene stack of 57 globally distributed benthic δ^{18}O records, Paleoceanography, 20, PA1003, doi:10.1029/2004PA001071, 2005.
Lisitzin, A. P.: Sea ice and iceberg sedimentation in the ocean: recent and past, Springer-Verlag, Berlin, 563 pp., 2002.

CPD
8, 6135–6198, 2012

Mahowald, N. M., Baker, A. R., Bergametti, G., Brooks, N., Duce, R. A., Jickells, D., Kubilay, N., Prospero, J. M., and Tegen, I.: Atmospheric global dust cycle and iron inputs to the ocean, Global Biogeochem. Cy., 19, GB4025, doi:10.1029/2004GB002402, 2005.

Malakhov, M. I., Gorbarenko, S. A., Malakhova, G. Y., Harada, N., Vasilenko, Y. P., Bosin, A. A., Goldberg, E. L., and Derkachev, A. N.: Petromagnetic parameters of bottom sediments as indicators of the climatic and environmental changes in the central zone of the Sea of Okhotsk during the last 350 kyr, Russ. Geol. Geophys., 50, 973–982, doi:10.1016/j.rgg.2009.10.006, 2009.

Mantua, N. J., Hare, S. R., Zhang, Y., Wallace, J. M., and Francis, R. C.: A Pacific interdecadal climate oscillation with impacts on salmon production, B. Am. Meteorol. Soc., 78, 1069–1079, 1997.

Marchitto, T. M., Lynch-Stieglitz, J., and Hemming, S. R.: Deep Pacific $CaCO_3$ compensation and glacial-interglacial atmospheric CO_2, Earth Planet. Sc. Lett., 231, 317–336, 2005.

Matul, A., Abelmann, A., Tiedemann, R., Kaiser, A., and Nürnberg, D.: Late Quaternary polycystine radiolarian datum events in the Sea of Okhotsk, Geo-Mar. Lett., 22, 25–32, 2002.

Max, L., Riethdorf, J.-R., Tiedemann, R., Smirnova, M., Lembke-Jene, L., Fahl, K., Nürnberg, D., Matul, A., and Mollenhauer, G.: Sea surface temperature variability and sea-ice extent in the subarctic northwest Pacific during the past 15,000 years, Paleoceanography, 27, PA3213, doi:10.1029/2012PA002292, 2012.

McDonald, D., Pedersen, T. F., and Crusius, J.: Multiple late Quaternary episodes of exceptional diatom production in the Gulf of Alaska, Deep-Sea Res. Pt. II, 46, 2993–3017, 1999.

McKay, J. L., Pedersen, T. F., and Kienast, S. S.: Organic carbon accumulation over the last 16 kyr off Vancouver Island, Canada: evidence for increased marine productivity during the deglacial, Quaternary Sci. Rev., 23, 261–281, 2004.

McLennan, S. M.: Sediments and soils: chemistry and abundances. in: Rock Physics and Phase Relations: a Handbook of Physical Constants, edited by: Ahrens, T. J., AGU Reference Shelf 3, AGU, Washington, 8–20, 1995.

Menviel, L., Timmermann, A., Elison Timm, O., Mouchet, A., Abe-Ouchi, A., Chikamoto, M. O., Harada, N., Ohgaito, R., and Okazaki, Y.: Removing the North Pacific halocline: effects on global climate, ocean circulation and the carbon cycle, Deep-Sea Res. Pt. II, 61–64, 106–113, 2012.

Middelburg, J. J., Soetaert, K., and Herman, P. M. J.: Empirical relationships for use in global diagenetic models, Deep-Sea Res. Pt. I, 44, 327–344, 1997.

CPD
8, 6135–6198, 2012

Müller, P.: C/N ratios in Pacific deep-sea sediments: effect of inorganic ammonium and organic nitrogen compounds sorbed by clays, Geochim. Cosmochim. Ac., 41, 765–776, 1977.
Müller, P. and Schneider, R.: An automated leaching method for the determination of opal in sediments and particulate matter, Deep-Sea Res. Pt. I, 40, 425–444, 1993.
Murray, R. W., Leinen, M., and Knowlton, C. W.: Links between iron input and opal deposition in the Pleistocene equatorial Pacific Ocean, Nat. Geosci., 5, 270–274, 2012.
Nakatsuka, T., Watanabe, K., Handa, N., Matsumoto, E., and Wada, E.: Glacial to interglacial surface nutrient variations of Bering deep basins recorded by δ^{13}C and δ^{15}N of sedimentary organic matter, Paleoceanography, 10, 1047–1061, 1995.
Nameroff, T. J., Calvert, S. E., and Murray, J. W.: Glacial-interglacial variability in the eastern tropical North Pacific oxygen minimum zone recorded by redox-sensitive trace metals, Paleocanography, 19, PA1010, doi:10.1029/2003PA000912, 2004.
Narita, H., Sato, M., Tsunogai, S., Murayama, M., Ikehara, M., Nakatsuka, T., Wakatsuchi, M., Harada, N., and Ujiié, Y.: Biogenic opal indicating less productive northwestern North Pacific during the glacial ages, Geophys. Res. Lett., 29, 1732, doi:10.1029/2001GL014320, 2002.
Nelson, D. M., Tréguer, P., Brzezinski, M. A., Leynaert, A., and Quéguiner, B.: Production and dissolution of biogenic silica in the ocean: revised global estimates, comparison with regional data and relationship to biogenic sedimentation, Global Biogeochem. Cy., 9, 359–372, 1995.
Niebauer, H. J.: Effects of El Nino–Southern Oscillation and North Pacific weather patterns on interannual variability in the subarctic Bering Sea, J. Geophys. Res., 93, 5051–5068, 1988.
Niebauer, H. J.: Variability in Bering Sea ice cover as affected by a regime shift in the North Pacific in the period 1947–1996, J. Geophys. Res., 103, 27717–27737, 1998.
Niebauer, H. J., Alexander, V., and Henrichs, S. M.: A time-series study of the spring bloom at the Bering Sea ice edge I. Physical processes, chlorophyll and nutrient chemistry, Cont. Shelf Res., 15, 1859–1877, 1995.
Niebauer, H. J., Bond, N. A., Yakunin, L. P., and Plotnikov, V. V.: An update on the climatology and sea ice of the Bering Sea, in: Dynamics of the Bering Sea, edited by: Loughlin, T. R. and Ohtani, K., University of Alaska Sea Grant, Fairbanks, Alaska, 29–59, 1999.
North Greenland Ice Core Project members: High-resolution record of Northern Hemisphere climate extending into the last interglacial period, Nature, 431, 147–151, 2004.
Nürnberg, C. C.: Bariumfluss und Sedimentation im südlichen Südatlantik – Hinweise auf Produktivitätsänderungen im Quartär, GEOMAR Reports 38, Research Center for Marine Geosciences (GEOMAR), Kiel, 105 pp., 1995.

CPD
8, 6135–6198, 2012

Nürnberg, C. C., Bohrmann, G., Schlüter, M., and Frank, M.: Barium accumulation in the Atlantic sector of the Southern Ocean: results from 190,000-year records, Paleoceanography, 12, 594–603, 1997.
Nürnberg, D. and Tiedemann, R.: Environmental change in the Sea of Okhotsk during the last 1.1 million years, Paleoceanography, 19, PA4011, doi:10.1029/2004PA001023, 2004.
Nürnberg, D., Wollenburg, I., Dethleff, D., Eicken, H., Kassens, H., Letzig, T., Reimnitz, E., and Thiede, J.: Sediments in Arctic sea ice: implications for entrainment, transport and release, Mar. Geol., 119, 185–214, 1994.
Nürnberg, D., Dethleff, D., Tiedemann, R., Kaiser, A., and Gorbarenko, S. A.: Okhotsk Sea ice coverage and Kamchatka glaciation over the last 350 ka – evidence from ice-rafted debris and planktonic δ^{18}O, Palaeogeogr. Palaeocl., 310, 191–205, 2011.
Ohkushi, K., Itaki, T., and Nemoto, N.: Last glacial-Holocene change in intermediate-water ventilation in the northwestern Pacific, Quaternary Sci. Rev., 22, 1477–1484, 2003.
Ohkushi, K., Uchida, M., Ahagon, N., Mishima, T., and Kanematsu, T.: Glacial intermediate water ventilation in the northwestern Pacific based on AMS radiocarbon dating, Nucl. Instrum. Meth. B, 223–224, 460–465, 2004.
Okada, M., Takagi, M., Narita, H., and Takahashi, K.: Chronostratigraphy of sediment cores from the Bering Sea and the subarctic Pacific based on paleomagnetic and oxygen isotopic analyses, Deep-Sea Res. Pt. II, 52, 2092–2109, 2005.
Okazaki, Y., Takahashi, K., Asahi, H., Katsuki, K., Hori, J., Yasuda, H., Sagawa, Y., and Tokuyama, H.: Productivity changes in the Bering Sea during the late Quaternary, Deep-Sea Res. Pt. II, 52, 2150–2162, 2005.
Okazaki, Y., Timmermann, A., Menviel, L., Harada, N., Abe-Ouchi, A., Chikamoto, M. O., Mouchet, A., and Asahi, H.: Deepwater formation in the North Pacific during the Last Glacial Maximum, Science, 329, 200–204, 2010.
Orians, K. J. and Bruland, K. W.: The biogeochemistry of aluminium in the Pacific Ocean, Earth Planet. Sc. Lett., 78, 397–410, 1986.
Ortiz, J. D., O'Connell, S. B., DelViscio, J., Dean, W., Carriquiry, J. D., Marchitto, T., Zheng, Y., and van Geen, A.: Enhanced marine productivity off western North America during warm climate intervals of the past 52 k.y., Geology, 32, 521–524, 2004.
Overland, J. E., Adams, J. M., and Bond, N. A.: Decadal variability of the Aleutian Low and its relation to high-latitude circulation, J. Climate, 12, 1542–1548, 1999.

CPD
8, 6135–6198, 2012

Overland, J. E., Bond, N. A., and Adams, J. M.: The relation of surface forcing of the Bering Sea to large-scale climate patterns, Deep-Sea Res. Pt. II, 49, 5855–5868, 2002.
Paillard, D., Labeyrie, L., and Yiou, P.: Macintosh program performs time-series analysis, EOS T. Am. Geophys. Un., 77, p. 379, doi:10.1029/96EO00259, 1996.
Pondaven, P., Ragueneau, O., Tréguer, P., Hauvespre, A., Dezileau, L., and Reyss, J. L.: Resolving the "opal paradox" in the Southern Ocean, Nature, 405, 168–172, 2000.
Pushkar, V. S., Roof, S. R., Cherepanova, M. V., Hopkins, D. M., and Brigham-Grette, J.: Paleogeographic and paleoclimatic significance of diatoms from middle Pleistocene marine and glaciomarine deposits on Baldwin Peninsula, northwestern Alaska, Palaeogeogr. Palaeocl., 152, 67–85, 1999.
Pye, K.: Aeolian dust and dust deposits, Academic Press, London, 334 pp., 1987.
Ragueneau, O., Tréguer, P., Leynaert, A., Anderson, R. F., Brzezinski, M. A., DeMaster, D. J., Dugdale, R. C., Dymond, J., Fischer, G., Francois, R., Heinze, C., Maier-Reimer, E., Martin-Jézéquel, V., Nelson, D. M., and Quéguiner, B.: A review of the Si cycle in the modern ocean: recent progress and missing gaps in the application of biogenic opal as a paleoproductivity proxy, Global Planet. Change, 26, 317–365, 2000.
Rasmussen, S. O., Andersen, K. K., Svensson, A. M., Steffensen, J. P., Vinther, B. M., Clausen, H. B., Siggaard-Andersen, M.-L., Johnsen, S. J., Larsen, L. B., Dahl-Jensen, D., Bigler, M., Röthlisberger, R., Fischer, H., Goto-Azuma, K., Hansson, M. E., and Ruth, U.: A new Greenland ice core chronology for the last glacial termination, J. Geophys. Res., 111, D06102, doi:10.1029/2005JD006079, 2006.
Redfield, A. C., Ketchum, B. H., and Richards, F. A.: The influence of organisms on the composition of seawater, in: The Sea, vol. 2, edited by: Hill, M. N., Wiley-Interscience, New York, 26–77, 1963.
Reed, R. K., Khen, G. V., Stabeno, P. J., and Verkhunov, A. V.: Water properties and flow over the deep Bering Sea basin, summer 1991, Deep-Sea Res. Pt. I, 40, 2325–2334, 1993.
Rella, S. F., Tada, R., Nagashima, K., Ikehara, M., Itaki, T., Ohkushi, K., Sakamoto, T., Harada, N., and Uchida, M.: Abrupt changes of intermediate water properties on the northeastern slope of the Bering Sea during the last glacial and deglacial period, Paleoceanography, 27, PA3203, doi:10.1029/2011PA002205, 2012.
Richter, T., van der Gaast, S., Koster, B., Vaars, A., Gieles, R., de Stigter, H., De Haas, H., and van Weering, T.: The Avaatech XRF core scanner: technical description and applications to NE Atlantic sediments, Geol. Soc. Spec. Publ., 267, 39–50, 2006.

CPD
8, 6135–6198, 2012

Riethdorf, J.-R., Max, L., Nürnberg, D., Lembke-Jene, L., and Tiedemann, R.: Deglacial development of (sub) sea surface temperature and salinity in the subarctic northwest Pacific: implications for upper-ocean stratification, Paleoceanography, in review, 2012.

Ronov, A. B. and Migdisov, A. A.: Geochemical history of the crystalline basement and the sedimentary cover of the Russian and North American platforms, Sedimentology, 16, 137–185, 1971.

Rösler, H. J. and Lange, H.: Geochemical Tables, Elsevier, New York, 468 pp., 1972.

Sagawa, T. and Ikehara, K.: Intermediate water ventilation change in the subarctic northwest Pacific during the last deglaciation, Geophys. Res. Lett., 35, L24702, doi:10.1029/2008GL035133, 2008.

Sarnthein, M., Stattegger, K., Dreger, D., Erlenkeuser, H., Grootes, P., Haupt, B. J., Jung, S., Kiefer, T., Kuhnt, W., Pflaumann, U., Schäfer-Neth, C., Schulz, H., Schulz, M., Seidov, D., Simstich, J., van Kreveld, S., Vogelsang, E., Völker, A., and Weinelt, M.: Fundamental modes and abrupt changes in North Atlantic circulation and climate over the last 60 ky – concepts, reconstruction and numerical modeling, in: The Northern North Atlantic: a Changing Environment, edited by: Schäfer, P., Ritzrau, W., Schlüter, M., and Thiede, J., Springer, Berlin, 365–410, 2001.

Sarnthein, M., Grootes, P. M., Kennett, J. P., and Nadeau, M.-J.: ^{14}C reservoir ages show deglacial changes in ocean currents and carbon cycle, in: Past and Future Changes of the Oceanic Meridional Overturning Circulation: Mechanisms and Impacts, edited by: Schmittner, A., Chiang, J. C. H., and Hemming, S. R., AGU Monograph Series 173, AGU, Washington, DC, 175–196, 2007.

Sato, M. M., Narita, H., and Tsunogai, S.: Barium increasing prior to opal during the last termination of glacial ages in the Okhotsk Sea sediments, J. Oceanogr., 58, 461–467, 2002.

Schlitzer, R.: Ocean Data View, http://odv.awi.de (last access: 6 August 2012), 2011.

Schmitz, B.: The TiO_2/Al_2O_3 ratio in the Cenozoic Bengal abyssal fan sediments and its use as a paleostream energy indicator, Mar. Geol., 76, 195–206, 1987.

Schneider, R. R., Price, B., Müller, P. J., Kroon, D., and Alexander, I.: Monsoon related variations in Zaire (Congo) sediment load and influence of fluvial silicate supply on marine productivity in the east equatorial Atlantic during the last 200,000 years, Paleoceanography, 12, 463–481, 1997.

Seki, O., Kawamura, K., Nakatsuka, T., Ohnishi, K., Ikehara, M., and Wakatsuchi, M.: Sediment core profiles of long-chain n-alkanes in the Sea of Okhotsk: enhanced transport of terrestrial

CPD
8, 6135–6198, 2012

organic matter from the last deglaciation to the early Holocene, Geophys. Res. Lett., 30, 1001, doi:10.1029/2001GL014464, 2003.
Shackleton, N. J. and Hall, M. A.: Oxygen and carbon isotope stratigraphy of Deep Sea Drilling Project Hole 552A: Plio-Pleistocene glacial history, in: Initial Reports DSDP, 81, edited by: Roberts, D. G., Schnitker, D., Backman, J., Baldauf, J. G., Desprairies, A., Homrighausen, R., Huddlestun, P., Kaltenback, A. J., Krumsiek, K. A. O., Morton, A. C., Murray, J. W., Westberg-Smith, J., and Zimmermann, H. B., US Govt. Printing Office, Washington, 599–609, doi:10.2973/dsdp.proc.81.116.1984, 1984.
Shigemitsu, M., Narita, H., Watanabe, Y. W., Harada, N., and Tsunogai, S.: Ba, Si, U, Al, Sc, La, Th, C and $^{13}C/^{12}C$ in a sediment core in the western subarctic Pacific as proxies of past biological production, Mar. Chem., 106, 442–455, 2007.
Sigman, D. M. and Boyle, E. A.: Glacial/interglacial variations in atmospheric carbon dioxide, Nature, 407, 859–869, 2000.
Sigman, D. M., Jaccard, S. L., and Haug, G. H.: Polar ocean stratification in a cold climate, Nature, 428, 59–63, 2004.
Sigman, D. M., Hain, M. P., and Haug, G. H.: The polar ocean and glacial cycles in atmospheric CO_2 concentration, Nature, 466, 47–55, 2010.
Springer, A. M., McRoy, C. P., and Flint, M. V.: The Bering Sea green belt: shelf-edge processes and ecosystem production, Fish. Oceanogr., 5, 205–223, 1996.
Stabeno, P. J., Schumacher, J. D., and Ohtani, K.: The physical oceanography of the Bering Sea, in: Dynamics of the Bering Sea, edited by: Loughlin, T. R. and Ohtani, K., University of Alaska Sea Grant, Fairbanks, Alaska, 1–28, 1999.
Stein, R.: Arctic Ocean sediments: processes, proxies, and paleoenvironment, in: Developments in Marine Geology, vol. 2, edited by: Chamley, H., Elsevier, Amsterdam, 592 pp., 2008.
Széréméta, N., Bassinot, F., Balut, Y., Labeyrie, L., and Pagel, M.: Oversampling of sedimentary series collected by giant piston corer: evidence and corrections based on 3.5-kHz chirp profiles, Paleoceanography, 19, PA1005, doi:10.1029/2002PA000795, 2004.
Takahashi, K.: The Bering and Okhotsk Sea: modern and past paleoceanographic changes and gateway impact, J. Asian Earth Sci., 16, 49–58, 1998.
Takahashi, K.: Paleoceanographic changes and present environment of the Bering Sea, in: Dynamics of the Bering Sea, edited by: Loughlin, T. R. and Ohtani, K., University of Alaska Sea Grant, Fairbanks, Alaska, 365–385, 1999.

CPD
8, 6135–6198, 2012

Takahashi, K.: The Bering Sea and paleoceanography, Deep-Sea Res. Pt. II, 52, 2080–2091, 2005.
Takahashi, K., Fujitani, N., and Yanada, M.: Long term monitoring of particle fluxes in the Bering Sea and the central subarctic Pacific Ocean, 1990–2000, Progr. Oceanogr., 55, 95–112, 2002b.
Takahashi, T., Sutherland, S. C., Sweeney, C., Poisson, A., Metzl, N., Tilbrook, B., Bates, N., Wanninkhof, R., Feely, R. A., Sabine, C., Olafsson, J., and Nojiri, Y.: Global sea–air CO_2 flux based on climatological surface ocean pCO_2 and seasonal biological and temperature effects, Deep-Sea Res. Pt. II, 49, 1601–1622, 2002a.
Tanaka, S. and Takahashi, K.: Late Quaternary paleoceanographic changes in the Bering Sea and the western subarctic Pacific based on radiolarian assemblages, Deep-Sea Res. Pt. II, 52, 2131–2149, 2005.
Taylor, S. R.: Abundance of chemical elements in the continental crust: a new table, Geochim. Cosmochim. Ac., 28, 1273–1285, 1964.
Taylor, S. R. and McLennan, S. M.: The geochemical evolution of the continental crust, Rev. Geophys., 33, 241–265, 1995.
Taylor, S. R., McLennan, S. M., and McCulloch, M. T.: Geochemistry of loess, continental crust composition and crustal model ages, Geochim. Cosmochim. Ac., 47, 1897–1905, 1983.
Ternois, Y., Kawamura, L., Keigwin, L., Ohkouchi, N., and Nakatsuka, T.: A biomarker approach for assessing marine and terrigenous inputs to the sediments of Sea of Okhotsk for the last 27,000 years, Geochim. Cosmochim. Ac., 65, 791–802, 2001.
Thunell, R. C., Varela, R., Llano, M., Collister, J., Muller-Karger, F., and Bohrer, R.: Organic carbon fluxes, degradation, and accumulation in an anoxic basin: sediment trap results from the Cariaco Basin, Limnol. Oceanogr., 45, 300–308, 2000.
Tjallingii, R., Röhl, U., Kölling, M., and Bickert, T.: Influence of the water content on X-ray fluorescence core-scanning measurements in soft marine sediments, Geochem. Geophy. Geosy., 8, Q02004, doi:10.1029/2006GC001393, 2007.
Tomczak, M. and Godfrey, J. S.: Regional oceanography: an introduction, Elsevier Science Ltd., Oxford, 391 pp., 1994.
Tyrrell, T., Merico, A., Waniek, J. J., Wong, C. S., Metzl, N., and Whitney, F.: Effect of seafloor depth on phytoplankton blooms in high-nitrate, low-chlorophyll (HNLC) regions, J. Geophys. Res., 110, G02007, doi:10.1029/2005JG000041, 2005.

CPD
8, 6135–6198, 2012

van Geen, A., Zheng, Y., Bernhard, J. M., Cannariato, K. G., Carriquiry, J., Dean, W. E., Eakins, B. W., Ortiz, J. D., and Pike, J.: On the preservation of laminated sediments along the western margin of North America, Paleoceanography, 18, 1098, doi:10.1029/2003PA000911, 2003.

Waelbroek, C., Labeyrie, L., Michel, E., Duplessy, J. C., McMannus, J. F., Lambeck, K., Balbon, E., and Labracherie, M.: Sea-level and deep water temperature changes derived from benthic foraminifera isotopic records, Quaternary Sci. Rev., 21, 295–305, 2002.

Wang, Y. J., Cheng, H., Edwards, R. L., An, Z. S., Wu, J. Y., Shen, C.-C., and Dorale, J. A.: A high-resolution absolute-dated Late Pleistocene monsoon record from Hulu cave, China, Science, 294, 2345–2348, 2001.

Wang, Y., Cheng, H., Edwards, R. L., Kong, X., Shao, X., Chen, S., Wu, J., Jiang, X., Wang, X., and An, Z.: Millennial- and orbital-scale changes in the East Asian monsoon over the past 224,000 years, Nature, 451, 1090–1093, 2008.

Warren, B.: Why is no deepwater formed in the North Pacific?, J. Mar. Res., 41, 327–347, 1983.

Wedepohl, K. H.: Environmental influences on the chemical composition of shales and clays, in: Physics and Chemistry of the Earth, edited by: Ahrens, L., Press, K., Runcorn, S., and Urey, H., Pergamon Press, Oxford, 307–333, 1971.

Yarincik, K. M., Murray, R. W., and Peterson, L. C.: Climatically sensitive eolian and hemipelagic deposition in the Cariaco Basin, Venezuela, over the past 578,000 years: results from Al/Ti and K/Al, Paleoceanography, 15, 210–228, 2000.

Yasonov, P. G., Nourgaliev, D. C., Bourov, B. V., and Heller, F.: A modernized coercivity spectrometer, Geol. Carpath., 49, 224–226, 1998.

Yasuda, I.: The origin of the North Pacific intermediate water, J. Geophys. Res., 102, 893–909, 1997.

Zhang, J., Woodgate, R., and Moritz, R.: Sea ice response to atmospheric and oceanic forcing in the Bering Sea, J. Phys. Oceanogr., 40, 1729–1747, 2010.

Zheng, Y., van Geen, A., Anderson, R. F., Gardner, J. V., and Dean, W. E.: Intensification of the northeast Pacific oxygen minimum zone during the Bölling-Alleröd warm period, Paleoceanography, 15, 528–536, 2000.

Ziegler, M., Jilbert, T., de Lange, G. J., Lourens, L. J., and Reichart, G.-J.: Bromine counts from XRF scanning as an estimate of the marine organic carbon content of sediment cores, Geochem. Geophy. Geosy., 9, Q05009, doi:10.1029/2007GC001932, 2008.

CPD
8, 6135–6198, 2012

Table 1. Site information.

Core	Latitude	Longitude	Depth (m b.s.l.)	Recovery (m)
SO201-2-77KL	56° 19.83′ N	170° 41.98′ E	2135	11.78
SO201-2-85KL	57° 30.30′ N	170° 24.77′ E	968	18.13
SO201-2-101KL	58° 52.52′ N	170° 41.45′ E	630	18.32

CPD
8, 6135–6198, 2012

Table 2. Statistics of parameters approximating marine productivity.

Parameter	SO201-2-77KL		SO201-2-85KL		SO201-2-101KL	
	Avg.	StDev.	Avg.	StDev.	Avg.	StDev.
TOC (wt. %)	0.85	0.30	0.96	0.36	0.88	0.16
[C/N]a	13.0	2.9	11.9	1.6	12.4	1.6
Opal (wt. %)	9.5	9.7	3.3	3.2	2.9	1.3
$CaCO_3$ (wt. %)	1.9	3.2	1.9	2.2	1.2	0.7
Ba_{bio} [1] (ppm)	733	330	436	141	260	85
P_{New} [2] ($g C m^{-2} yr^{-1}$)	50.6	47.5	34.9	21.5	29.9	21.1
PP [3] ($g C m^{-2} yr^{-1}$)	131.9	54.2	113.1	34.8	102.9	37.6

[1] Via Al using the global average Ba/Al of pelitic rocks of 6.5 $mg g^{-1}$ (Wedepohl, 1971).
[2] After Nürnberg (1995).
[3] After Eppley and Peterson (1979).

CPD
8, 6135–6198, 2012

Table 3. Statistics of parameters approximating terrigenous matter supply.

Parameter	SO201-2-77KL		SO201-2-85KL		SO201-2-101KL	
	Avg.	StDev.	Avg.	StDev.	Avg.	StDev.
> 63 µm (wt. %)	5.6	3.1	7.5	5.4	7.9	7.4
%Siliciclastics	88.9	8.8	94.1	4.4	94.9	1.5
%Terrigen (Al-norm.)[1]	82.7	10.2	88.2	7.3	89.3	5.9
%Terrigen (Ti-norm.)[2]	76.6	9.6	84.4	8.4	83.8	6.2
[Ti] ($\mu mol\,g^{-1}$)	86.4	10.9	95.2	9.5	94.5	7.0
[Fe] ($\mu mol\,g^{-1}$)	762	112	792	96	740	90
[Al] ($\mu mol\,g^{-1}$)	2578	316	2751	227	2783	185

[1] Using [Al] = 3117 $\mu mol\,g^{-1}$ of average continental crust (Taylor and McLennan, 1995).
[2] Using [Ti] = 112.8 $\mu mol\,g^{-1}$ of average continental crust (Taylor and McLennan, 1995).

CPD
8, 6135–6198, 2012

Table 4. Ranges, averages and variability of atomic elemental ratios in cores SO201-2-77KL, -85KL, and -101KL.

	SO201-2-77KL		SO201-2-85KL		SO201-2-101KL	
	Al/Ti	Fe/Al	Al/Ti	Fe/Al	Al/Ti	Fe/Al
Average	29.9	0.30	29.0	0.29	29.5	0.26
StDev.	1.5	0.03	1.5	0.02	1.2	0.02
Maximum	34.1	0.34	32.3	0.36	32.4	0.30
Minimum	24.9	0.17	22.1	0.23	27.8	0.21

CPD
8, 6135–6198, 2012

Table A1. Age-depth points for core SO201-2-77KL. Ages < 20 ka BP and AMS-^{14}C ages have been derived from Max et al. (2012) and calendar ages are given with 1σ-ranges (in ka BP).

Core	Depth (cm)	Cal. Age (ka BP)	Approach
SO201-2-77KL	6	2.0[1]	color b* vs. color b* (SO201-2-12KL)
SO201-2-77KL	49	7.6[1]	color b* vs. color b* (SO201-2-12KL)
SO201-2-77KL	103	10.3	Carbonate spike 1
SO201-2-77KL	105.5	/	AMS-^{14}C dating (10.05–10.15)[2]
SO201-2-77KL	115.5	/	AMS-^{14}C dating (11.17–11.22)[3]
SO201-2-77KL	116	11.2	Carbonate spike 2
SO201-2-77KL	126	11.6	color b* vs. NGRIP
SO201-2-77KL	155.5	12.62	AMS-^{14}C dating (12.61–12.73)
SO201-2-77KL	168.5	13.83	AMS-^{14}C dating (13.82–13.97)
SO201-2-77KL	180.5	14.75	AMS-^{14}C dating (14.50–14.95)
SO201-2-77KL	187	15.1	color b* vs. color b* (85KL)
SO201-2-77KL	221	17.0	color b* vs. color b* (85KL)
SO201-2-77KL	258	21.5	Ca/Ti vs. Ca/Ti (85KL)
SO201-2-77KL	381	35.5	color b* vs. color b* (85KL)
SO201-2-77KL	393	37.2	color b* vs. color b* (85KL)
SO201-2-77KL	443	42.0	color b* vs. color b* (85KL)
SO201-2-77KL	478	46.9	color b* vs. color b* (85KL)
SO201-2-77KL	596	59.5	color b* vs. color b* (85KL)
SO201-2-77KL	656	64.7	Ca/Ti vs. Ca/Ti (85KL)
SO201-2-77KL	722	70.8	color b* vs. color b* (85KL)
SO201-2-77KL	736	72.3	color b* vs. color b* (85KL)
SO201-2-77KL	777	76.4	color b* vs. color b* (85KL)
SO201-2-77KL	796	77.7	color b* vs. color b* (85KL)
SO201-2-77KL	849	84.7	color b* vs. color b* (85KL)
SO201-2-77KL	898	89.1	Ca/Ti vs. Ca/Ti (85KL)
SO201-2-77KL	986	101.5	Ca/Ti vs. Ca/Ti (85KL)
SO201-2-77KL	1043	108.0	color b* vs. color b* (85KL)
SO201-2-77KL	1100	116.9	color b* vs. color b* (85KL)
SO201-2-77KL	1120	120.2	color b* vs. color b* (85KL)
SO201-2-77KL	1166	124.2	color b* vs. color b* (85KL)

[1] Uncertain age.
[2] Used to define carbonate spike 1 (see Max et al., 2012).
[3] Used to define carbonate spike 2 (see Max et al., 2012).

CPD
8, 6135–6198, 2012

Table A2. Age-depth points for core SO201-2-85KL. Ages < 20 ka BP and AMS-^{14}C ages have been derived from Max et al. (2012) and calendar ages are given with 1σ-ranges (in ka BP).

Core	Depth (cm)	Cal. Age (ka BP)	Approach
SO201-2-85KL	1	7.6[1]	color b* vs. color b* (SO201-2-12KL)
SO201-2-85KL	26.5	/	AMS-^{14}C dating (10.38–10.51)[2]
SO201-2-85KL	28	10.3	Carbonate spike 1
SO201-2-85KL	44	11.2	Carbonate spike 2
SO201-2-85KL	45.5	/	AMS-^{14}C dating (10.79–10.97)[3]
SO201-2-85KL	52	11.6	color b* vs. NGRIP
SO201-2-85KL	60.5	13.10	AMS-^{14}C dating (13.10–13.22)
SO201-2-85KL	70.5	13.87	AMS-^{14}C dating (13.67–13.89)
SO201-2-85KL	77	14.6	color b* vs. NGRIP
SO201-2-85KL	82	14.9	color b* vs. NGRIP
SO201-2-85KL	95.5	15.84	AMS-^{14}C dating (15.80–15.82)
SO201-2-85KL	135.5	19.90	AMS-^{14}C dating (19.58–19.90)
SO201-2-85KL	155.5	23.78	AMS-^{14}C dating (23.71–24.19)
SO201-2-85KL	209	26.2	Transfer of AMS-^{14}C age from core 101KL, but not well constrained
SO201-2-85KL	266	35.5	color b* vs. NGRIP
SO201-2-85KL	292	36.6	color b* vs. NGRIP
SO201-2-85KL	305	38.2	color b* vs. NGRIP
SO201-2-85KL	350	41.9	RPI vs. PISO-1500 (Laschamp)
SO201-2-85KL	363	43.4	color b* vs. NGRIP
SO201-2-85KL	398	46.9	color b* vs. NGRIP
SO201-2-85KL	433	48.4	color b* vs. NGRIP
SO201-2-85KL	463	51.7	color b* vs. NGRIP
SO201-2-85KL	490	54.2	color b* vs. NGRIP
SO201-2-85KL	567	59.5	color b* vs. NGRIP
SO201-2-85KL	657	64.0	color b* vs. NGRIP
SO201-2-85KL	675	65.0	RPI vs. PISO-1500 (Norwegian–Greenland Sea)
SO201-2-85KL	796	72.3	color b* vs. NGRIP
SO201-2-85KL	853	76.4	color b* vs. NGRIP
SO201-2-85KL	876	77.8	color b* vs. NGRIP
SO201-2-85KL	937	84.7	color b* vs. NGRIP
SO201-2-85KL	976	87.7	color b* vs. NGRIP
SO201-2-85KL	1006	91.7	color b* vs. NGRIP
SO201-2-85KL	1100	104.1	color b* vs. NGRIP
SO201-2-85KL	1149	108.0	color b* vs. NGRIP
SO201-2-85KL	1180	110.2	color b* vs. NGRIP
SO201-2-85KL	1210	113.3	color b* vs. NGRIP
SO201-2-85KL	1224	114.8	color b* vs. NGRIP
SO201-2-85KL	1240	117.0	RPI vs. PISO-1500 (Blake)
SO201-2-85KL	1280	125.0	color b* vs. Sanbao δ^{18}O (MIS5.5 climate optimum)
SO201-2-85KL	1300	130.0[4]	SMP vs. LR04 (MIS 5/6 Boundary)
SO201-2-85KL	1320	132.0	color b* vs. Sanbao δ^{18}O (HE11)
SO201-2-85KL	1365	135.0	color b*, Ca/Ti vs. Sanbao δ^{18}O
SO201-2-85KL	1530	151.0	color b*, Ca/Ti vs. Sanbao δ^{18}O
SO201-2-85KL	1600	159.0	RPI vs. PISO-1500
SO201-2-85KL	1735	174.0[4]	SMP vs. LR04 (MIS6 minimum)
SO201-2-85KL	1813	181.8[5]	Extrapolation

[1] Uncertain age; [2] used to define carbonate spike 1 (see Max et al., 2012); [3] used to define carbonate spike 2 (see Max et al., 2012); [4] scalar magnetic properties (SMP) correlated with MIS boundaries of LR04; [5] by extrapolation using linear sedimentation rate (LSR).

CPD
8, 6135–6198, 2012

Table A3. Age-depth points for core SO201-2-101KL. Ages < 20 ka BP and AMS-^{14}C ages have been derived from Max et al. (2012) and calendar ages are given with 1σ-ranges (in ka BP).

Core	Depth (cm)	Cal. Age (ka BP)	Approach
SO201-2-101KL	4	12.9	Ca/Ti vs. Ca/Ti (85KL)
SO201-2-101KL	10.5	13.56	AMS-^{14}C dating (13.69–13.84)
SO201-2-101KL	41	14.6	color b* vs. NGRIP
SO201-2-101KL	67	15.4	color b* vs. NGRIP
SO201-2-101KL	90.5	17.25	AMS-^{14}C dating (17.17–17.51)
SO201-2-101KL	110.5	18.95	AMS-^{14}C dating (19.54–19.92)
SO201-2-101KL	140	23.78	Transfer of AMS-^{14}C age from core 85KL
SO201-2-101KL	190.5	25.74	AMS-^{14}C dating (25.88–26.35)
SO201-2-101KL	234	28.6	color b* vs. NGRIP
SO201-2-101KL	249	30.3	color b* vs. NGRIP
SO201-2-101KL	260.5	32.0	AMS-^{14}C dating (32.12–33.54)
SO201-2-101KL	274	33.5	Ca/Ti vs. Ca/Ti (85KL)
SO201-2-101KL	280	35.1	Ca/Ti vs. Ca/Ti (85KL)
SO201-2-101KL	284	35.7	Ca/Ti vs. Ca/Ti (85KL)
SO201-2-101KL	302	36.9	Ca/Ti vs. Ca/Ti (85KL)
SO201-2-101KL	349	39.7	Ca/Ti vs. Ca/Ti (85KL)
SO201-2-101KL	387	43.1	Ca/Ti vs. Ca/Ti (85KL)
SO201-2-101KL	454	46.9	Ca/Ti vs. Ca/Ti (85KL)
SO201-2-101KL	514	51.6	Ca/Ti vs. Ca/Ti (85KL)
SO201-2-101KL	650	56.6	Ca/Ti vs. Ca/Ti (85KL)
SO201-2-101KL	685	57.8	Ca/Ti vs. Ca/Ti (85KL)
SO201-2-101KL	723	59.7	Ca/Ti vs. Ca/Ti (85KL)
SO201-2-101KL	799	64.1	Ca/Ti vs. Ca/Ti (85KL)
SO201-2-101KL	923	71.7	Ca/Ti vs. Ca/Ti (85KL)
SO201-2-101KL	1005	76.4	color b* vs. color b* (85KL)
SO201-2-101KL	1023	77.8	color b* vs. color b* (85KL)
SO201-2-101KL	1092	84.4	Ca/Ti vs. Ca/Ti (85KL)
SO201-2-101KL	1142	89.1	Ca/Ti vs. Ca/Ti (85KL)
SO201-2-101KL	1236	94.5	color b* vs. color b* (85KL)
SO201-2-101KL	1301	103.5	color b* vs. color b* (85KL)
SO201-2-101KL	1526	116.0	Benthic δ^{18}O vs. LR04
SO201-2-101KL	1585	125.0	color b* vs. Sanbao δ^{18}O (MIS5.5 climate optimum)
SO201-2-101KL	1625	130.0	Ca/Ti vs. Ca/Ti (85KL)
SO201-2-101KL	1635	132.0	color b* vs. Sanbao δ^{18}O (HE11)
SO201-2-101KL	1657	133.1	Ca/Ti vs. Ca/Ti (85KL)
SO201-2-101KL	1684	134.6	color b* vs. color b* (85KL)
SO201-2-101KL	1738	141.8	Ca/Ti vs. Ca/Ti (85KL)
SO201-2-101KL	1765	145.1	color b* vs. color b* (85KL)
SO201-2-101KL	1804	147.8	Ca/Ti vs. Ca/Ti (85KL)
SO201-2-101KL	1832	149.7[1]	Extrapolation

[1] By extrapolation using linear sedimentation rate (LSR).

CPD
8, 6135–6198, 2012

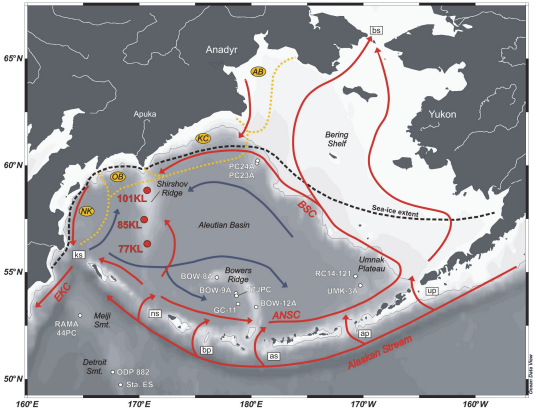

Fig. 1. Bathymetric map of the study area with 250 m isobathe. Locations of sediment cores SO201-2-77KL, -85KL, and -101KL are marked by red dots. White dots indicate reference records referred to in this study. Meiji Seamount: RAMA44PC (Keigwin et al., 1992). Detroit Seamount: ODP Site 882 (Jaccard et al., 2005), KH99-3 Sta. ES (Narita et al., 2002). Bowers Ridge: GC-11 (Gorbarenko, 1996; Gorbarenko et al., 2005, 2010), KH99-3-BOW-8A, -9A, and -12A (Katsuki and Takahashi, 2005; Okada et al., 2005; Okazaki et al., 2005; Tanaka and Takahashi, 2005), HLY02-02-17JPC (Brunelle et al., 2007, 2010). Umnak Plateau: KH99-3-UMK-3A (Okada et al., 2005; Okazaki et al., 2005; Tanaka and Takahashi, 2005), RC14-121 (Cook et al., 2005). Northern slope: MR06-04-PC23A and -PC24A (Itaki et al., 2009; Khim et al., 2010; Kim et al., 2011; Rella et al., 2012). Dashed black line indicates average maximum sea-ice extent (after Niebauer et al., 1999; Zhang et al., 2010). Dotted yellow line shows mineralogical provinces of coarse silts (after Lisitzin, 2002). The surface and deep circulation patterns (after Stabeno et al., 1999) are indicated by red and blue arrows, respectively. Mineralogial provinces: NK = Northern Kamchatka, OB = Olyutorskii Bay, KC = Koryak Coast, AB = Anadyr Bay. Surface currents: ANSC = Aleutian North Slope Current, BSC = Bering Slope Current, EKC = East Kamchatka Current. Straits: ks = Kamchatka Strait, ns = Near Strait, bp = Buldir Pass, as = Amchitka Strait, ap = Amukta Pass, up = Unimak Pass, bs = Bering Strait. This map was generated with "Ocean Data View" (Schlitzer, 2011).

CPD
8, 6135–6198, 2012

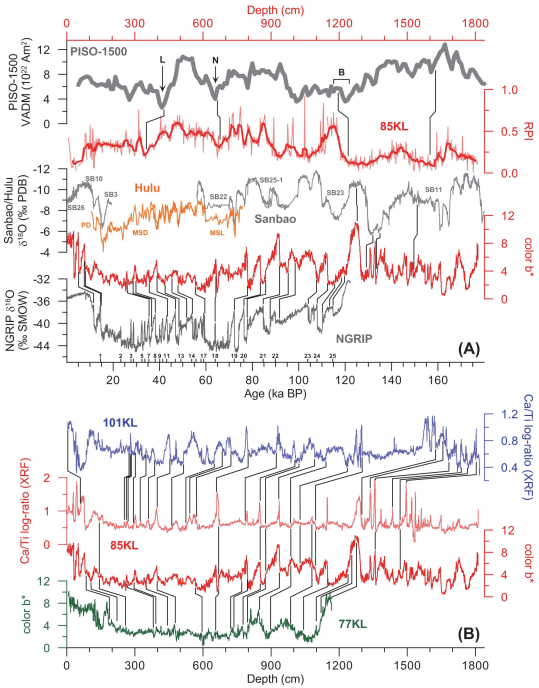

Fig. 2. (A) Correlation of sediment core SO201-2-85KL with the PISO-1500 (thick grey line) paleomagnetic reference record (Channell et al., 2009) based on relative paleointensity (RPI, smoothed by a 5-point-running average), as well as with the Sanbao (grey lines) and Hulu (orange lines) stalagmite δ^{18}O records (Wang et al., 2001, 2008) and the NGRIP δ^{18}O record (NGRIP members, 2004; GICC05 timescale, Rasmussen et al., 2006) based on color b*. Black lines mark correlation lines. The Laschamp (L), Norwegian–Greenland Sea (N), and Blake (B) paleomagnetic events are indicated. Bottom numbers mark D-O events. **(B)** Intercore correlation of sediment cores SO201-2-77KL (green) and -101KL (blue) with core -85KL (red) is based on color b* and XRF Ca/Ti log-ratio records.

CPD
8, 6135–6198, 2012

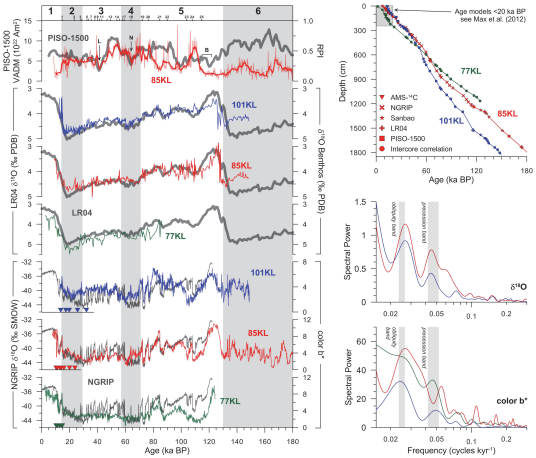

Fig. 3. Left: comparison of proxy records from sediment cores SO201-2-77KL (green lines), -85KL (red lines), and -101KL (blue lines) with published reference records (grey lines). Age models are primarily based on the graphic correlation between color b* records and the NGRIP δ^{18}O record (NGRIP members, 2004; GICC05 timescale, Rasmussen et al., 2006). Benthic δ^{18}O values from *U. peregrina* and *U. auberiana* are in agreement with the global reference stack LR04 (Lisiecki and Raymo, 2005). Relative paleointensity (RPI, smoothed by a 5-point-running average) recorded in core 85KL compares with the paleomagnetic reference record PISO-1500 (Channell et al., 2009). L, N, and B mark the Laschamp, Norwegian–Greenland Sea, and Blake paleomagnetic events. Absolute age control is provided by AMS-^{14}C-dating (coloured triangles; see Max et al., 2012). Top numbers indicate Marine Isotope Stages (boundaries after Lisiecki and Raymo, 2005) and D-O events. Upper right: age versus depth diagram showing the age-depth points and their underlying stratigraphic approach (see also Appendix A). Lower right: spectral analysis of benthic δ^{18}O and color b* records performed in the time domain revealed dominant cyclicities that lie within the frequency bands of Earth's obliquity and precession cycles.

CPD
8, 6135–6198, 2012

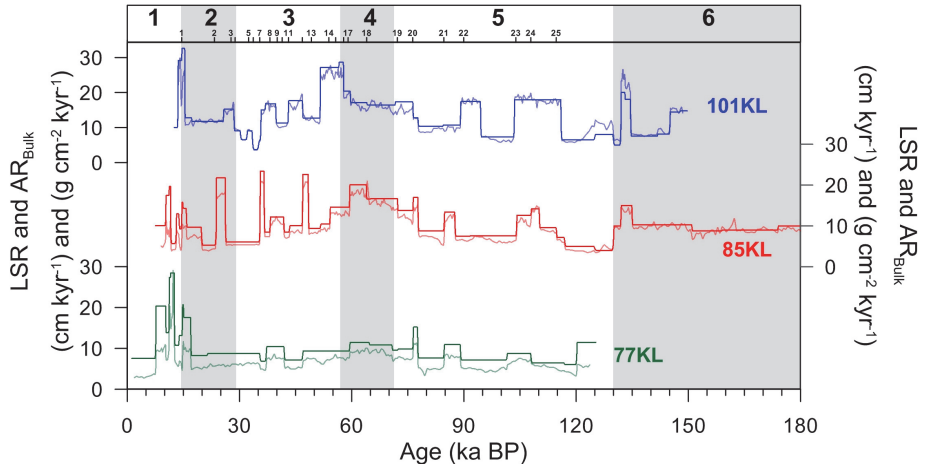

Fig. 4. Linear sedimentation rates (LSR) and bulk accumulation rates (AR_{Bulk}; transparent lines) of sediment cores SO201-2-77KL (green), -85KL (red), and -101KL (blue). LSR and AR_{Bulk} are plotted on the same scale.

CPD
8, 6135–6198, 2012

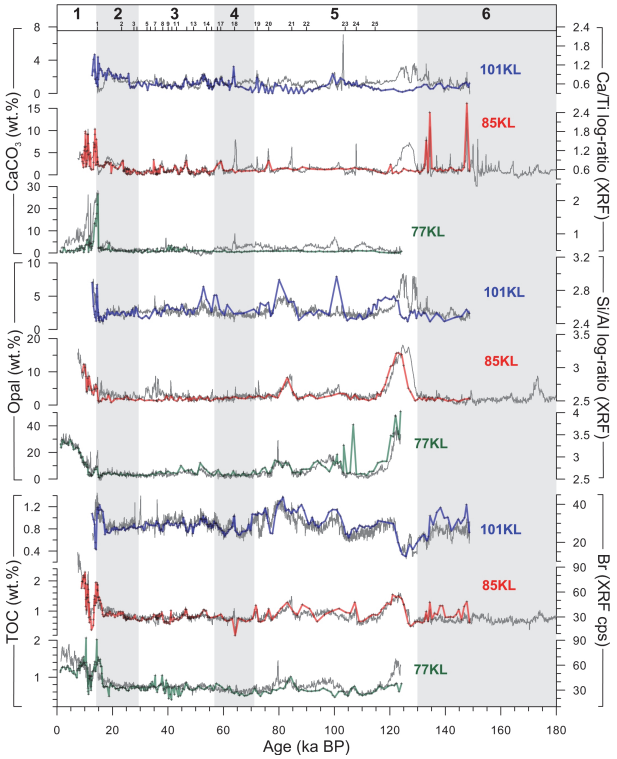

Fig. 5. Proxy records from cores SO201-2-77KL (green lines), -85KL (red lines), and -101KL (blue lines) approximating changes in marine productivity over the last 180 kyr. Concentrations of TOC, biogenic opal, and $CaCO_3$ (coloured lines), are shown in comparison to XRF records of Br (in cps), as well as XRF Si/Al and Ca/Ti log-ratios (underlying grey lines), respectively.

CPD
8, 6135–6198, 2012

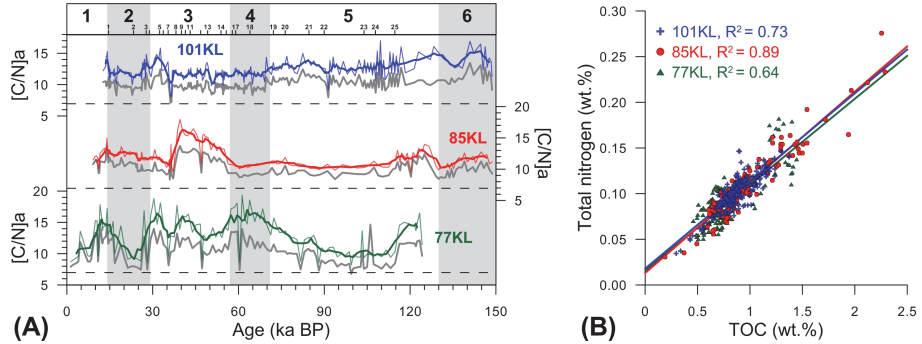

Fig. 6. (A) Atomic [C/N]a ratios (coloured lines, smoothed by a 5-point-running average), corrected for inorganic nitrogen compounds, and uncorrected C/N ratios (underlying grey lines) for cores SO201-2-77KL (green line), -85KL (red line), and -101KL (blue line) over the past 150 kyr. Dashed horizontal lines mark a C/N ratio of 7. Lower values represent typically marine-derived organic matter. **(B)** Linear regressions between TOC and TN conducted for each core result in intercept-values that reflect the amount of inorganic nitrogen (TIN). TN contents corrected for TIN were subsequently used to calculate [C/N]a ratios.

CPD
8, 6135–6198, 2012

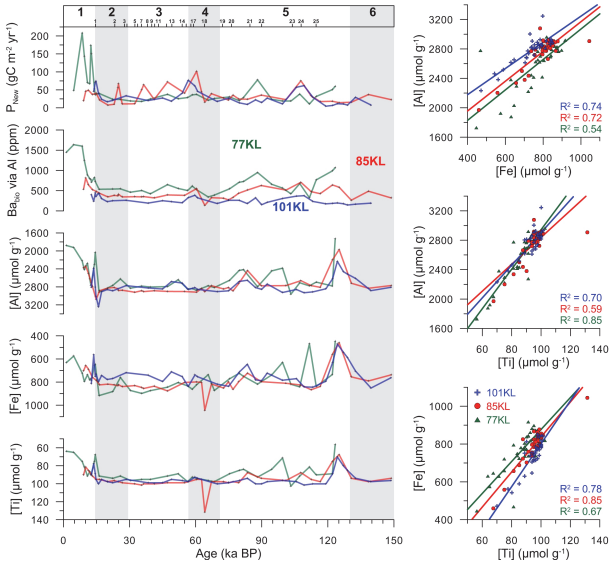

Fig. 7. Left: concentrations of lithogenous elements Ti, Fe, and Al (angular brackets), as well as of biogenic barium (Ba_{bio}) and new production (P_{New}) for the last 150 kyr. P_{New} was calculated from Ba_{bio} using the equation of Nürnberg (1995): $P_{New} = 3.56 \times F\,Ba_{bio}^{1.504} \times z^{-0.0937}$, where $F\,Ba_{bio} = AR\,Ba_{bio}/[0.209 \times \log_{10}(AR_{Bulk} \times 1000) - 0.213]$ (Dymond et al., 1992), and z = water depth (in m). $F\,Ba_{bio}$ is the flux of biogenic Ba to the seafloor (in $\mu g\,cm^{-2}\,yr^{-1}$), $AR\,Ba_{bio}$ is the accumulation rate of biogenic Ba (in $mg\,cm^{-2}\,kyr^{-1}$). Note that for records of [Ti], [Fe], and [Al] Y-axes are inverted. Right: correlation between lithogenous elements and respective linear correlation coefficients (R^2) indicate a shared terrigenous source of these elements.

CPD
8, 6135–6198, 2012

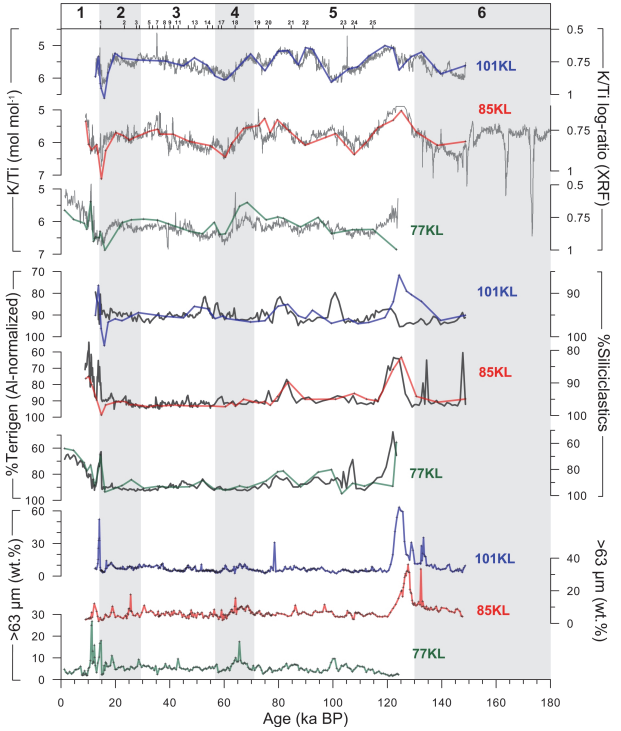

Fig. 8. Records approximating changes in terrigenous matter supply over the past 180 kyr. Relative contents of coarse material (> 63 µm), terrigenous matter (normalized to Al concentrations of continental crust; Taylor and McLennan, 1995), and atomic K/Ti ratios (coloured lines), in comparison to relative amounts of siliciclastics, and XRF K/Ti log-ratios (underlying grey lines) for cores SO201-2-77KL (green lines), -85KL (red lines), and -101KL (blue lines). Note that all Y-axes are inverted, except for > 63 µm.

CPD
8, 6135–6198, 2012

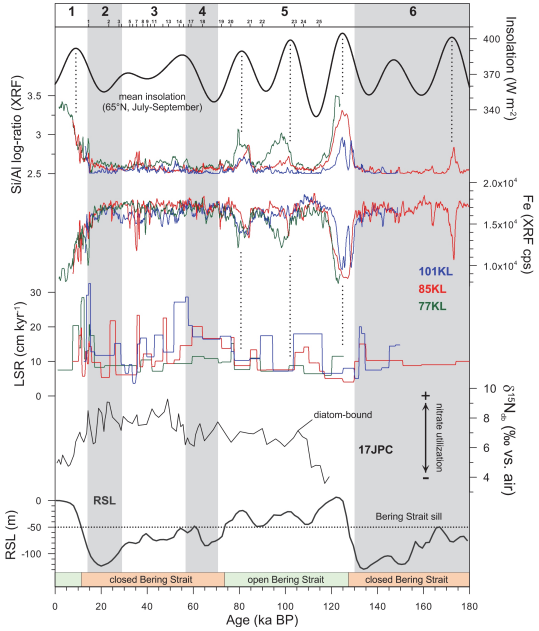

Fig. 9. Records of XRF Si/Al log-ratios reflecting changes in biogenic opal concentrations (marine productivity), XRF records of Fe (in cps) reflecting relative changes in terrigenous matter supply, and linear sedimentation rates (LSR) at sites SO201-2-77KL (green lines), -85KL (red lines), and -101KL (blue lines) for the last 180 kyr. Logging data are smoothed by 5-point-running averages. Relative sea-level (RSL) is after Waelbroek et al. (2002). The dashed horizontal line indicates the sill depth of the Bering Strait (~ 50 m). Summer insolation at 65° N (July/August) was calculated after Laskar (2004). Records of diatom-bound nitrogen isotope ratios ($\delta^{15}N_{db}$), assumed to reflect changes in nitrate utilization, are shown for Bowers Ridge core 17JPC (Brunelle et al., 2007). Comparison of these records suggests that marine productivity and terrigenous matter supply are subject to external forcing by summer insolation and sea-level changes.

CPD
8, 6135–6198, 2012